Scientific Reports

https://doi.org/10.1038/s41598-026-53535-y

Article in Press

# Fractional-order Klein-Gordon nonlocal model for thermo-elasto-diffusion in porous medium

Received: 10 February 2026

Accepted: 12 May 2026

Published online: 27 May 2026

Cite this article as: Sur A., Alosaimi M., Singhal A. *et al.* Fractional-order Klein-Gordon nonlocal model for thermo-elasto-diffusion in porous medium. *Sci Rep* (2026). https://doi.org/10.1038/s41598-026-53535-y

Abhik Sur, Moataz Alosaimi, Abhinav Singhal, Murat Yaylacı & Soumik Das

We are providing an unedited version of this manuscript to give early access to its findings. Before final publication, the manuscript will undergo further editing. Please note there may be errors present which affect the content, and all legal disclaimers apply.

If this paper is publishing under a Transparent Peer Review model then Peer Review reports will publish with the final article.

ARTICLE IN PRESS

© The Author(s) 2026. **Open Access** This article is licensed under a Creative Commons Attribution-NonCommercial-NoDerivatives 4.0 International License, which permits any non-commercial use, sharing, distribution and reproduction in any medium or format, as long as you give appropriate credit to the original author(s) and the source, provide a link to the Creative Commons licence, and indicate if you modified the licensed material. You do not have permission under this licence to share adapted material derived from this article or parts of it. The images or other third party material in this article are included in the article's Creative Commons licence, unless indicated otherwise in a credit line to the material. If material is not included in the article's Creative Commons licence and your intended use is not permitted by statutory regulation or exceeds the permitted use, you will need to obtain permission directly from the copyright holder. To view a copy of this licence, visit http://creativecommons.org/licenses/by-nc-nd/4.0/.

ARTICLE IN PRESS

# Fractional-Order Klein-Gordon Nonlocal Model for Thermo-Elasto-Diffusion in Porous Medium

**Abhik Sur[1], Moataz Alosaimi[2], Abhinav Singhal[3], Murat Yaylacı[4], Soumik Das[5,*]**

*[1]Department of Mathematics, Sister Nivedita University, Kolkata, West Bengal, India*
*[2]Department of Mathematics and Statistics, College of Science, Taif University, P.O. Box 11099, Taif 21944, Saudi Arabia*
*[3]Department of Mathematics, Christ University, Bangalore, India*
*[4]Department of Civil Engineering, Recep Tayyip Erdogan University, 53100, Rize, Turkey*
*[5]School of Physical Sciences, Amrita Vishwa Vidyapeetham, Mysuru Campus, Karnataka, India*
*[*]Corresponding author, Email: soumikdas@my.amrita.edu , soumikdas1993@gmail.com*

**Abstract:**

Classical heat conduction and thermoelastic theories are often inadequate for describing transport processes in modern micro and nano-scale materials, as they assume instantaneous propagation and neglect memory and nonlocal effects. This limitation becomes particularly important in applications such as semiconductor devices and porous structures subjected to rapid thermal and chemical loading. To address this issue, the present study develops a generalized thermo-elasto-diffusion model for porous medium by incorporating fractional-order heat conduction and Klein-Gordon-type nonlocal dynamics. The model extends the classical Lord–Shulman framework through a set of fractional-order modified models derived using an analogy with viscoelastic behavior, allowing both memory effects and spatial interactions to be captured through intrinsic time and length scales. Analytical solutions are obtained in the Laplace domain and numerically inverted using Zakian's algorithm to evaluate the transient response of displacement, temperature, chemical potential, and stress fields. The results show that fractional-order parameters and nonlocal effects significantly influence wave propagation and heat transfer, especially near boundaries and in regions with strong microstructural interactions. Overall, the proposed framework provides a more realistic and physically consistent description of coupled thermo-mechanical processes, offering useful insights for the design and analysis of advanced porous and semiconductor materials under extreme conditions.

ARTICLE IN PRESS

**Keywords:** Fractional-order derivative; porous material; modified Lord-Shulman model, Klein-Gordon operator; heat and mass transfer

**Abbreviations:**

| Symbols | Definitions | Symbols | Definitions |
|---|---|---|---|
| $s_{ij}$, $s_{ij}^{L}$ | Nonlocal and local stress tensors | $s_i$, $s_i^{L}$ | Nonlocal and local equilibrated stress vectors |
| $z$, $z^{L}$ | Nonlocal and local intrinsic equilibrated body force | $S^{*}$ | Entropy |
| $P$ | Chemical potential | $C$ | Mass concentration |
| $u$ | Displacement | $\gamma$ | Void volume fraction |
| $\varphi$ | Temperature | $\lambda, \mu$ | Lame's constants |
| $\xi, A_1, a_1$ | Void parameters | $b, n$ | Thermal parameters |
| $m, a_2$ | Diffusion parameters | $r$ | Parameter measuring thermo-diffusion effect |
| $s$ | Parameter measuring diffusion effect | $e_{ij}$ | Strain tensor |
| $x$ | Spatial nonlocality parameter | $t$ | Temporal nonlocality parameter |
| $d$ | Coefficient of diffusivity | $\kappa$ | Thermal conductivity |
| $w, u$ | Time delay parameters | $\alpha$ | Fractional-order parameter |
| $t$ | Time | $\varphi_0$ | Reference temperature |

## 1. Introduction

ARTICLE IN PRESS

According to traditional theories of thermal transport [1-2], the heat flux is linearly proportional to the temperature gradient. However, this classical formulation leads to the non-physical prediction of infinite thermal propagation speed, where temperature disturbances are instantaneously felt at distant points. Addressing this inconsistency has driven the evolution of advanced heat conduction models. With the growing importance of thermomechanical analysis in modern technologies such as MEMS/NEMS, FGMs, TBCs, and ultrafast laser applications. The inclusion of non-Fourier effects has become essential [3–5]. To overcome the limitations of Fourier's law, Carlo Cattaneo [6] and Pierre Vernotte [7] proposed the hyperbolic heat conduction model (CV), introducing a time derivative of heat flux to account for finite propagation speed. This framework was extended by D. Y. Tzou [8] through the dual-phase-lag (DPL) model, incorporating distinct delays for heat flux and temperature gradient, although its thermodynamic consistency remains debated. The Lord and Shulman (LS) theory [9] integrates the CV model with classical elasticity, while the Green and Lindsay (GL) theory [10] introduces relaxation effects in stress and entropy relations. Furthermore, the Green and Naghdi (GN) model [11,12] employs thermal displacement as a fundamental variable. Building on these developments, recent studies have explored fractional-order models [13], memory-dependent formulations [14], and nonlocal theories [15].

The fundamental principles of diffusion theory describe the spontaneous movement of particles from regions of high concentration to low concentration. Over recent decades, this framework has been significantly refined to address complex engineering applications across geophysical and technological domains, including semiconductor design, integrated resistor fabrication, and petroleum reservoir management. In such processes, thermal energy plays a crucial role in enhancing particle mobility, giving rise to thermodiffusion, which establishes a strong coupling between temperature gradients, mass transport, and mechanical deformation in

ARTICLE IN PRESS

elastic solids. Within this coupled system, variations in thermal or chemical fields induce mechanical responses, while structural changes, in turn, influence heat and mass transfer. This interplay is particularly important in nano-scale systems, such as nano-electromechanical systems (NEMS) [16], where accurate modeling of thermo-elastodiffusive behavior is essential for ensuring device performance and reliability under non-uniform thermal conditions.

However, classical diffusion models based on Fick's law suffer from the non-physical prediction of infinite propagation speeds. Early formulations, such as those by Nowacki [17], were limited by this drawback. To overcome this issue, Sherief et al. [18] introduced a generalized thermodiffusion framework incorporating a relaxation time to ensure finite wave propagation. Building on this foundation, Sherief and Saleh [19] analyzed thermo-chemical interactions in a one-dimensional half-space, while Aoudi [20] extended the analysis to medium with spherical cavities. Further studies have explored wave propagation characteristics in porous thermodiffusive solids [21] and examined the effects of rotation and gravity using Dual-Phase-Lag (DPL) and Lord-Shulman (LS) theories [22]. More recently, Dutta and co-workers [23,24] advanced the field by developing generalized thermoelastic diffusion models that integrate Lord-Shulman and Moore–Gibson–Thompson frameworks.

Over the past few decades, fractional calculus [25,26] has emerged as a powerful mathematical framework for modeling systems exhibiting spatial nonlocality, memory effects, and hereditary behavior. Its versatility has led to widespread applications across fields such as electromagnetics, control engineering, quantum-scale modeling, and materials science. In particular, modern technological materials [27–29], characterized by complex microstructural responses, are effectively described using fractional-order operators due to their ability to capture long-range temporal correlations. Significant contributions by various researchers [30–32] have advanced this

ARTICLE IN PRESS

field by integrating fractional-order concepts into multi-temperature and nonlocal thermoelastic theories, offering deeper insights into wave propagation in generalized thermomechanical systems. This line of research has been further extended by Das and co-workers [33–36], who investigated energy transport mechanisms in piezo-thermo-electric medium using memory-dependent and phase-lag formulations, revealing intricate couplings between mechanical, thermal, and electrical fields that are not captured by classical integer-order models.

The historical trajectory of nonlocal continuum mechanics began with the foundational interaction frameworks established by Edelen and Laws [37], which challenged the limitations of classical local theories. These early concepts were subsequently refined by Eringen and Edelen [38], who integrated thermodynamic equilibrium and global balance laws to create a cohesive theory for materials governed by long-range interatomic interactions. This body of work became the primary pillar for modern nonlocal elasticity, an essential tool for investigating size-dependent behaviors at the micro- and nano-scales [39]–[42]. However, the widely utilized differential model introduced by Eringen has recently been subjected to rigorous re-examination. Critical mathematical inconsistencies were uncovered by Romano [43] and Kaplunov [44,45], whose counterexamples cast doubt on the universal reliability of the classical formulation. In response to these theoretical gaps, a weakly nonlocal elastic framework within spatial domains was introduced by Anh and Vinh [30], enabling the study of surface wave dynamics at the interfaces of nonlocal structures. This line of inquiry was further extended by Anh’s research group [31] to analyze Rayleigh-type waves under impedance boundary conditions. Concurrently, a Klein–Gordon-type weakly nonlocal model for isotropic solids was developed by Lazar and Agiasofitou [32]. By replacing earlier Helmholtz-based theories with a system that incorporates both spatial and temporal scaling parameters, they significantly enhanced the

ARTICLE IN PRESS

model's descriptive power. The inclusion of temporal nonlocality is particularly noteworthy; it allows for the theoretical observation of frequency band gaps and optical branches in dispersion spectra—phenomena that remain hidden in strictly acoustic wave analysis.

Porous materials with internal cavities play a crucial role in engineering and natural sciences, with applications ranging from lightweight aerospace structures and thermal insulation to biological tissues and geological formations. The theoretical foundation for modeling such medium is the theory of elastic materials with voids, where the microstructure is characterized by the void volume fraction, defined as the ratio of the bulk density of the porous matrix to that of the solid material. This framework incorporates void effects directly into the kinematic variables and naturally reduces to classical elasticity in the absence of porosity. The linear and nonlinear formulations of this theory were established by Cowin and co-workers [49,50], who later showed that elastic materials with voids exhibit inherent viscoelastic behavior [51]. Further investigations by Puri and Cowin [52] demonstrated that such medium support one transverse and two coupled dilatational waves. Studies on wave propagation in porous layers by Dey et al. [53] revealed the existence of two distinct wave fronts associated with material rigidity and void distribution. More recently, Gupta et al. [54] applied the Green–Naghdi (GN-III) thermoelasticity framework to analyze deformation in rotating, exponentially graded medium with dual-porosity structures [55–58].

The motivation for the present study arises from the need for accurate and physically consistent models to describe thermo-mechanical behavior in micro- and nano-structured porous materials under rapid thermal and chemical loading [59-68]. Classical thermoelastic and diffusion theories fail to capture finite-speed wave propagation, long-range interactions, and memory-dependent transport. Although nonlocal elasticity and fractional-order models have advanced the field, they are typically developed

ARTICLE IN PRESS

separately and do not simultaneously incorporate spatial and temporal nonlocal effects within a unified thermo-elasto-diffusion framework [69-76]. In particular, the integration of Klein–Gordon-type spatiotemporal nonlocality into fractional-order thermoelastic diffusion models for porous medium with voids remains largely unexplored [77, 78].

To address this gap, the present study introduces a unified framework combining fractional-order heat conduction with Klein–Gordon-type nonlocal elasticity, capturing both memory effects and intrinsic length-scale interactions. The proposed Fractional-order Modified Lord-Shulman (FOMLS) model accounts for coupled spatial–temporal nonlocality and memory dependence. The main contributions include analytical solutions for the coupled field equations in a porous strip and an investigation of how void volume fraction and nonlocal parameters influence wave propagation. These results are relevant for applications such as thermal barrier coatings, MEMS/NEMS devices, and semiconductor sensors under ultrafast excitations. The remainder of the paper outlines the mathematical formulation, model development, problem setup, solution methodology using Laplace transforms and Zakian's inversion, validation, and discussion of results, followed by conclusions.

ARTICLE IN PRESS

## 2. Basic equations for spatiotemporal nonlocality

Consider a three-dimensional infinite elastic continuum occupying region $V$. When the medium experiences distributed body forces $F_i$, the motion equation derived from Newton's law takes the form

$$s_{ij,j}(\mathbf{x},t)+F_i(\mathbf{x},t)=\rho\ddot{u}_i(\mathbf{x},t), \quad (1)$$

where $s_{ij}$ is the nonlocal stress and $u_i$ being the displacement components. Considering the effect of both spatial and temporal nonlocal interactions, the constitutive law, motivated by analogies with the electrodynamics of continuous medium takes the following generalized form [48], [79]:

ARTICLE IN PRESS

$$s_{ij}(\mathbf{x},t)=\int_{-\infty}^{t}\int_{V}C_{ijkl}(\mathbf{x},t;\mathbf{x}',t')\,e_{kl}(\mathbf{x}',t')\,dV(\mathbf{x}')\,dt' \quad (2)$$

where $C_{ijkl}$ denotes the fourth-order elasticity tensor, satisfying the usual symmetry conditions, i.e. $C_{ijkl}=C_{jikl}, C_{ijkl}=C_{ijlk}$. The infinitesimal strain components relate to displacements through

$$e_{kl}=\frac{1}{2}\left(u_{k,l}+u_{l,k}\right).$$

The overall nonlocal mechanical response of the medium is governed by a tensor function $C_{ijkl}$ that incorporates the effects of spatial interactions. Thus, the dynamic equation including nonlocal contributions becomes

$$\frac{\partial}{\partial x_j}\int_{-\infty}^{t}\int_{V}C_{ijkl}(\mathbf{x},t;\mathbf{x}',t')\,e_{kl}(\mathbf{x}',t')\,dV(\mathbf{x}')\,dt'+F_i(\mathbf{x},t)=\rho\ddot{u}_i \quad (3)$$

To decouple nonlocal anisotropy from the material's inherent elastic anisotropy, the nonlocal tensor $C_{ijkl}(\mathbf{x}-\mathbf{x}',t-t')$ is represented as the product of a scalar kernel function $a(\mathbf{x}-\mathbf{x}',t-t')$ and the local anisotropic modulus tensor $C_{ijkl}$:

$$C_{ijkl}(\mathbf{x}-\mathbf{x}',t-t')=C_{ijkl}\,a(\mathbf{x}-\mathbf{x}',t-t'). \quad (4)$$

The scalar nonlocal kernel $a(\mathbf{x}-\mathbf{x}',t-t')$ accounts for both spatial and temporal dependencies, thereby embedding intrinsic length and time scale effects into the formulation. Hence, the nonlocal stress state is represented as an integral of the classical Cauchy stress tensor, weighted by a kernel function across both space and time:

$$s_{ij}(\mathbf{x},t)=\int_{-\infty}^{t}\int_{V}C_{ijkl}(\mathbf{x},t;\mathbf{x}',t')\,e_{kl}(\mathbf{x}',t')\,dV(\mathbf{x}')\,dt'=a(\mathbf{x},t)*s_{ij}^{L}(\mathbf{x},t),$$

where $*$ denotes the spatiotemporal convolution operator, signifying integration over both spatial and temporal dimensions.

For the special case of a homogeneous, isotropic solid, the nonlocal tensor simplifies to:

ARTICLE IN PRESS

ARTICLE IN PRESS

$$s_{ij}(x,t) = \int_{-\infty}^{t}\int_{V} a(|x-x'|,t-t')\, s^{L}_{ij}(x',t')\, dV(x')\, dt'. \quad (5)$$

Here the Cauchy stress tensor $\sigma^{L}_{ij} = \lambda e_{kk}\delta_{ij} + 2\eta e_{ij}$ retains its standard representation in terms of the Lamé parameters $\lambda$ and $\eta$. Eringen highlighted that matching the dispersion curves of plane waves with lattice dynamics observations serves as a benchmark for the reliability of the scalar nonlocal kernel. The scalar kernel can be written in terms of a linear differential operator $L$ by using the Green's function technique. The general representation of the kernel operator $L$ for an unbounded medium:

$$L\,a(|x-x'|,t-t') = \delta(x-x')\,\delta(t-t'). \quad (6)$$

Substituting the operator $L$ into equation (5) and invoking expression (6), we get the governing differential form:

$$L s_{ij} = s^{L}_{ij}. \quad (7)$$

Here, the Cauchy stress tensor $s^{L}_{ij}$ represents the nonhomogeneous term. This formulation clarifies that the scalar kernel function is identically the Green's function associated with the differential operator. Hence, the integral constitutive form given in (5) can equivalently be expressed in the differential form presented in (7). Assuming the operator $L$ possesses linearity with constant coefficients, the equation of motion (1) when combined with (7) yields:

$$L(\rho\,\partial_t^2 u_i) - \partial_j s^{L}_{ij} = L F_i. \quad (8)$$

The Helmholtz operator may be further extended to form a second-order dynamic hyperbolic differential operator [48], [79] represented as:

$$L \approx 1 - \ell^2\nabla^2 + \tau^2\frac{\partial^2}{\partial t^2}. \quad (9)$$

In this formulation, the Laplacian operator $\nabla^2$ defines spatial dispersion, while the parameter $\ell \in \mathbb{R}^{+}$ introduces the intrinsic length scale controlling the degree of spatial nonlocality. The constant $\ell = e_0 a_d$ corresponds to a material-dependent factor $e_0$, and $\tau \in \mathbb{R}^{+}$ represents the temporal scale associated with nonlocal delay effects. By defining a characteristic

ARTICLE IN PRESS

propagation velocity $c \in R^+$ as $c=\frac{l}{t}$, the hyperbolic operator $\mathcal{L}$ transforms into the well-known Klein–Gordon (KG) operator. According to Eringen, a plausible estimation of the characteristic length scale can be expressed as $l \simeq 0.39a$, where $a$ denotes the lattice constant. The nonlocal elasticity incorporated through the KG formulation introduces intrinsic spatial and temporal length scales that account for long-range interatomic interactions and microstructural heterogeneity. Specifically, the intrinsic length scale parameter is associated with the characteristic size of the microstructural features, such as pore size, grain size, or interatomic spacing. In porous thermoelastic materials, it can be interpreted as a measure of the interaction radius over which neighboring points influence each other. In a similar manner, the temporal nonlocal (delay) parameter reflects the finite time required for the material to respond to thermal or mechanical disturbances, capturing relaxation and memory effects.

From a physical standpoint, Klein-Gordon nonlocal dynamics arises from the need to incorporate finite-range spatial interactions and finite-speed temporal responses into continuum models. Unlike classical local elasticity, where the response at a point depends only on its immediate state, nonlocal formulations recognize that material behavior is influenced by neighboring regions due to long-range interatomic forces and microstructural heterogeneity.

## 3. Generalized heat conduction models

Drawing an analogy between heat conduction and viscoelastic behavior, thermal elasticity and thermal viscosity are modeled using elements that correspond to the elastic springs and dashpots in viscoelastic theory. When the concept of thermal displacement is defined as $\vartheta$ ($\dot{\vartheta} = \theta$, where $\theta$ is the temperature), its spatial gradient expressed as $\varpi = \nabla\vartheta$.

ARTICLE IN PRESS



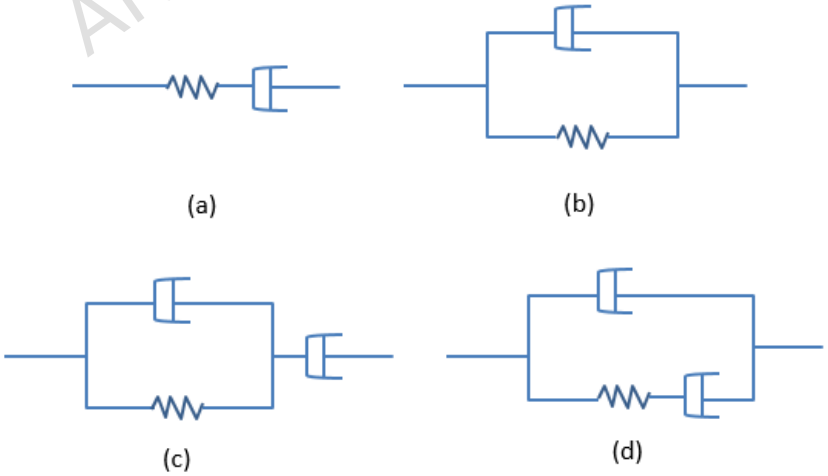

**Figure 1**: (a) Thermoelastic unit and (b) Thermo-viscoelastic unit.

As indicated in Fig. 1, the governing heat conduction relations for these thermal elastic and viscous components are formulated as [80]:

$$h = -k^{*}\nabla, \quad h = -k\nabla\dot{\delta}. \quad (10)$$

In this expression, $h$ signifies the heat flux vector, $k$ stands for the thermal conductivity coefficient, $u$ represents the relaxation time, and $k^{*}=\frac{k}{u}$ is a material-dependent parameter. In the present study, the correspondence between viscoelastic mechanical models and generalized heat conduction formulations, as initially proposed in [80], is further employed to derive extended analogies. This approach enables the development of more sophisticated generalized heat conduction models by combining thermal elastic and viscous elements in either series or parallel arrangements, as depicted in Fig. 2. On this basis, several modified forms of heat conduction models are constructed in the subsequent sections.

ARTICLE IN PRESS



ARTICLE IN PRESS

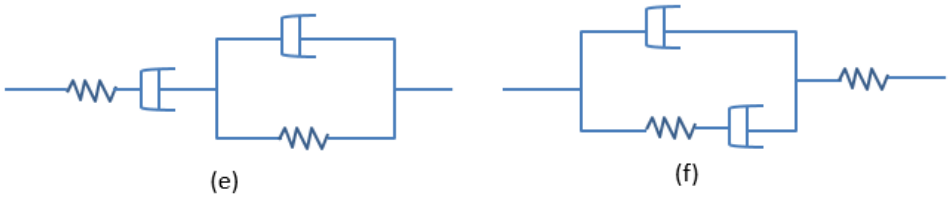



**Figure 2: (a)** Fractional-order Lord-Shulman **(**FOLS), **(b)** Fractional-order Green-Naghdi **(**FOGN), **(c)** Fractional-order modified Lord-Shulman-I **(**FOMLS-I)**, (d)** Fractional-order modified Lord-Shulman-II **(**FOMLS-II)**, (e)** Fractional-order modified Lord-Shulman-III **(**FOMLS-III)**,** and **(f)** Fractional-order modified Lord-Shulman-IV **(**FOMLS-IV) heat transfer models.

### 3.1 Fractional-order LS (FOLS) heat conduction model

Nowadays, the fractional heat conduction provides a powerful tool for modeling memory-dependent and anomalous transport processes. Classical Fourier-based models assume instantaneous heat flux response, which fails to describe heat transfer in materials exhibiting thermal relaxation, long memory, or non-Fickian diffusion. These fractional-order formulations propose a non-integer time derivative, which effectively captures the history-dependent evolution of thermal fields and allows for a more accurate description of sub-diffusive and super-diffusive heat transport. This is particularly important in porous medium, biological tissues, and in many physical systems, where heat transport is strongly influenced by internal structure and temporal memory effects. Engineering applications include thermal management in microelectronic devices, heat transfer in composite and porous insulation systems, and ultrafast laser–material interactions, where classical models fail to predict experimentally observed thermal responses.

Within the classical LS thermoelastic theory, the thermal elastic and thermal viscous elements are assumed to experience an identical heat flux, i.e.,

$$h = h_1 = h_2. \quad (11)$$

The overall thermal displacement is obtained by adding the thermal displacements contributed by each of the two constituent units

$$\varpi = \varpi_1 + \varpi_2. \quad (12)$$

ARTICLE IN PRESS

Among them,

$$h_1 = -k^* v_1, \; h_2 = -k v_2 \quad (13)$$

The preceding relationship gives rise to the formulation of the LS transfer model

$$\left(1 + \upsilon \frac{\partial}{\partial t}\right) h = -k \nabla q. \quad (14)$$

Following the methodology [57], a generalized fractional-order form of the LS heat conduction law is introduced as

$$\left(1 + \frac{\upsilon^\alpha}{\Gamma(\alpha+1)} \frac{\partial^\alpha}{\partial t^\alpha}\right) h = -k \nabla q. \quad (15)$$

The fractional-order parameter $\alpha$, defined as

$$\frac{\partial^\alpha f(x,z,t)}{\partial t^\alpha} = \begin{cases} f(x,z,t) - f(x,z,0), & \text{when } \alpha \to 0 \\ I^{1-\alpha} \dfrac{\partial f(x,z,t)}{\partial t}, & \text{when } 0 < \alpha < 1 \\ \dfrac{\partial f(x,z,t)}{\partial t}, & \text{when } \alpha = 1, \end{cases}$$

with

$$I^\alpha f(x,z,t) = \frac{1}{\Gamma(\alpha)} \int_0^t (t-s)^{\alpha-1} f(x,z,s)\, ds.$$

### 3.2 Fractional-order modified LS (FOMLS) heat conduction models

More general heat-conduction relations emerge from alternative series and parallel arrangements of thermal elastic and viscous elements. Based on the schematic framework depicted in Figure 2, four extended formulations—denoted as FOMLS-I, FOMLS-II, FOMLS-III, and FOMLS-IV—are subsequently developed.

#### 3.2.1 Fractional-order modified LS-I (FOMLS-I) heat conduction model (Series GN + Viscous Element)

The thermal displacement is additive, and a uniform heat flux is assumed, such that

$$\hbar = \hbar_1 = \hbar_2, \quad \varpi = \varpi_1 + \varpi_2. \quad (16)$$

For the GN model,

$$\upsilon_1 \dot{\hbar}_1 = -\kappa_1 \dot{\varpi}_1 - \kappa_1 \upsilon_1 \ddot{\varpi}_1. \quad (17)$$

For the viscous unit,

ARTICLE IN PRESS

$$h_2 = -k_2 \nabla\theta \quad (18)$$

Using (16)-(18), the generalized heat conduction equation for the MLS-I model can be formulated as follows

$$\frac{k_1}{k_2} h + u_1 \left(1 + \frac{k_1}{k_2}\right) \dot{h} = -k_1 \nabla\theta - k_1 u_1 \nabla\dot{\theta} \quad (19)$$

It is also consider that $k = k_1 = k_2, u = u_1$. Consequently, the above equation can be rearranged into the form

$$\left(1 + 2u \frac{\partial}{\partial t}\right) h = -k \left(1 + u \frac{\partial}{\partial t}\right) \nabla q \quad (20)$$

For FOMLS-I, equation (20) can be modified as

$$\left(1 + 2 \frac{\upsilon^{\alpha}}{\Gamma(\alpha+1)} \frac{\partial^{\alpha}}{\partial t^{\alpha}}\right) \hbar = -\kappa \left(1 + \frac{\upsilon^{\alpha}}{\Gamma(\alpha+1)} \frac{\partial^{\alpha}}{\partial t^{\alpha}}\right) \nabla\theta. \quad (21)$$

However, corresponding to the case when $\alpha \to 1$, we arrive at

$$\left(1 + 2\nu \frac{\partial}{\partial t}\right) \hbar = -\kappa \left(1 + \nu \frac{\partial}{\partial t}\right) \nabla\theta .$$

### 3.2.2 Fractional-order modified LS-II (FOMLS-II) heat conduction model (Parallel CV + Viscous Element)

The thermal displacement is common, and the heat fluxes are additive, such that

$$h = h_1 + h_2, \nu = \nu_1 = \nu_2. \quad (22)$$

For the LS model,

$$u_1 \dot{h}_1 + h_1 = -k_1 \nabla\nu_1 \quad (23)$$

For the viscous unit,

$$h_2 = -k_2 \nabla\dot{\nu}_2 \quad (24)$$

From equations (22) and (23), we have

$$u_1 \ddot{h} + \dot{h} = -u_1 k_2 \nabla\ddot{\nu} - (k_1 + k_2) \nabla\dot{\nu} \quad (25)$$

It is also consider that $k = k_1 = k_2, u = u_1$, equation (25) can be derived in the following form

ARTICLE IN PRESS

$$\left(1+\upsilon\frac{\partial}{\partial t}\right)\hbar=-k\left(2+\upsilon\frac{\partial}{\partial t}\right)\nabla q \ . \quad (26)$$

For FOMLS-II, equation (26) can be written as

$$\left(1+\frac{\upsilon^{\alpha}}{\Gamma(\alpha+1)}\frac{\partial^{\alpha}}{\partial t^{\alpha}}\right)\hbar=-k\left(2+\frac{\upsilon^{\alpha}}{\Gamma(\alpha+1)}\frac{\partial^{\alpha}}{\partial t^{\alpha}}\right)\nabla q. \quad (27)$$

However, corresponding to the case when $\alpha\to 1$, we arrive at

$$\left(1+\nu\ \frac{\partial}{\partial t}\right)\hbar=-\kappa\left(2+\nu\ \frac{\partial}{\partial t}\right)\nabla\theta\ .$$

### 3.2.3 Fractional-order modified LS-III (FOMLS-III) heat conduction model (Series CV + GN Combination)

The heat flux is common, and the thermal displacement is additive, such that

$$h=h_1=h_2,\ v=v_1+v_2.$$

Additionally, the model adheres to the relation

$$\hbar_1+\upsilon_1\dot{\hbar}_1=-\kappa_1\nabla\theta,\upsilon_2\dot{\hbar}_2=-\kappa_2\nabla\theta-\kappa_2\upsilon_2\nabla\dot{\theta}. \quad (28)$$

By combining the above-mentioned conditions, we arrive at the following expression

$$\frac{k_2}{k_1}h+\left(u_2+\frac{k_2}{k_1}u_1+\frac{k_2}{k_1}u_2\right)\dot{h}+\frac{k_2}{k_1}u_1u_2\ddot{h}=-k_2\nabla q-k_2u_2\nabla\dot{q}. \quad (29)$$

It is also consider that $k=k_1=k_2, u=u_1=u_2,$ equation (29) can be reformulated as follows:

$$\left(1+3u\frac{\partial}{\partial t}+u^2\frac{\partial^2}{\partial t^2}\right)h=-k\left(1+u\frac{\partial}{\partial t}\right)\nabla q. \quad (30)$$

For FOMLS-III, equation (30) can be modified as

$$\left(1+3\frac{\upsilon^{\alpha}}{\Gamma(\alpha+1)}\frac{\partial^{\alpha}}{\partial t^{\alpha}}+\frac{\upsilon^{2\alpha}}{\Gamma(2\alpha+1)}\frac{\partial^{2\alpha}}{\partial t^{2\alpha}}\right)\hbar=-k\left(1+\frac{\upsilon^{\alpha}}{\Gamma(\alpha+1)}\frac{\partial^{\alpha}}{\partial t^{\alpha}}\right)\nabla q. \quad (31)$$

However, corresponding to the case when $\alpha\to 1$, we arrive at

$$\left(1+3\nu\ \frac{\partial}{\partial t}+\frac{\nu^2}{2!}\ \frac{\partial^2}{\partial t^2}\right)\hbar=-\kappa\left(2+\nu\ \frac{\partial}{\partial t}\right)\nabla\theta\ .$$

ARTICLE IN PRESS

### 3.2.4 Fractional-order modified LS-IV (FOMLS-IV) heat conduction model (Series FOMLS-II + Thermoelastic Element)

The inclusion of an additional thermal elastic element introduces a further relaxation mechanism into the system

$$\left.\begin{aligned} &\hbar = \hbar_1 = \hbar_2, \qquad \varpi = \varpi_1 + \varpi_2, \\ &\hbar_1 + \upsilon_1 \dot{\hbar}_1 = -2\kappa_1 \nabla\theta - \kappa_1 \upsilon_1 \nabla\dot{\theta}, \dot{\hbar}_2 = -\kappa_2 \varpi_2. \end{aligned}\right\} \quad (32)$$

By combining the system of equations presented above, we derive the following result

$$\hbar + \left(u_1 + 2\frac{k_1}{k_2}u_2\right)\dot{\hbar} + \frac{k_1}{k_2}u_1 u_2 \ddot{\hbar} = -2k_1 \nabla q - k_1 u_1 \nabla \dot{q}. \quad (33)$$

Assuming consistent cell parameters, we attain

$$\left(1 + 3u\frac{\partial}{\partial t} + u^2 \frac{\partial^2}{\partial t^2}\right)\hbar = -k\left(2 + u\frac{\partial}{\partial t}\right)\nabla q. \quad (34)$$

For FOMLS-IV, equation (34) can be rewritten as

$$\left(1 + 3\frac{u^{\alpha}}{\Gamma(\alpha+1)}\frac{\partial^{\alpha}}{\partial t^{\alpha}} + \frac{u^{2\alpha}}{\Gamma(2\alpha+1)}\frac{\partial^{2\alpha}}{\partial t^{2\alpha}}\right)\hbar = -k\left(2 + \frac{u^{\alpha}}{\Gamma(\alpha+1)}\frac{\partial^{\alpha}}{\partial t^{\alpha}}\right)\nabla q. \quad (35)$$

However, corresponding to the case when $\alpha \to 1$, we arrive at

$$\left(1 + 3\nu\,\frac{\partial}{\partial t} + \frac{\nu^2}{2!}\,\frac{\partial^2}{\partial t^2}\right)\hbar = -\kappa\left(2 + \nu\,\frac{\partial}{\partial t}\right)\nabla\theta\,.$$

ARTICLE IN PRESS

## 4. Governing equations

The foundational governing equations for the linear framework of thermoelastic diffusion within porous structures were initially formulated by Aouadi [20]. This study expands upon their theory by incorporating extended Lord-Shulman thermoelasticity and integrating Klein-Gordon nonlocal elasticity theory [48].

- Stress-strain-temperature relations [55, 56]

$$\left(1 - \xi^2\nabla^2 + \tau^2\frac{\partial^2}{\partial t^2}\right)\sigma_{ij} = \sigma_{ij}^{L} = 2\eta e_{ij} + (\lambda e_{kk} + \gamma\psi - \beta\theta - \mu C)\delta_{ij}, \quad (36)$$

$$\left(1 - x^2\nabla^2 + t^2\frac{\partial^2}{\partial t^2}\right)s_i = (s_i)^{L} = A_1 y_{,i}, \quad (37)$$

ARTICLE IN PRESS

$$\left(1-\chi^2\nabla^2+t^2\frac{\partial^2}{\partial t^2}\right)\sigma_{kk}^{L}=\sigma^{L}=-\beta e_{kk}-\alpha_1\psi+\eta\theta+\alpha_2 C, \quad (38)$$

$$\left(1-\chi^2\nabla^2+t^2\frac{\partial^2}{\partial t^2}\right)rS^{*}=\left(rS^{*}\right)^{L}=be_{kk}+\eta\psi+a\theta+rC, \quad (39)$$

$$\left(1-\xi^2\nabla^2+\tau^2\frac{\partial^2}{\partial t^2}\right)P=P^{L}=-\mu e_{kk}-\tilde{\alpha}\psi-r\theta+sC. \quad (40)$$

- ***Equations of motion [55]***

$$s_{ij,j}^{L}+\left(1-\chi^2\nabla^2+t^2\frac{\partial^2}{\partial t^2}\right)F_i=\rho\left(1-\chi^2\nabla^2+t^2\frac{\partial^2}{\partial t^2}\right)\ddot{u}_i, \quad (41)$$

$$(\sigma_i)^{L}+\zeta^{L}+\rho\left(1-\xi^2\nabla^2+\tau^2\frac{\partial^2}{\partial t^2}\right)I_1^{*}=\chi\left(1-\xi^2\nabla^2+\tau^2\frac{\partial^2}{\partial t^2}\right)\ddot{\psi}. \quad (42)$$

- ***Energy scale equation [55]***

$$\rho q_0\dot{S}=-h_{i,i}, \quad (43)$$

$$\dot{C}=-m_{i,i}. \quad (44)$$

- ***Nonlocal FOMLS thermo-elasto-diffusion model***

By incorporating the Klein-Gordon nonlocal operator, the heat conduction and mass diffusion laws for all the thermo-elasto-diffusion models (FOLS, FOMLS-I, FOMLS-II, FOMLS-III, FOMLS-IV) are expressed in the following form

$$\left(1-\chi^2\nabla^2+t^2\frac{\partial^2}{\partial t^2}\right)B_1h_i=-E_1kq_{,i}, \quad (45)$$

$$\left(1-\chi^2\nabla^2+t^2\frac{\partial^2}{\partial t^2}\right)B_2m_i=-E_2dP_{,i}, \quad (46)$$

where the expressions of $B_i$ and $E_i$ are given in the Table 1.

| **Thermo-elasto-diffusion models** | $B_i$ | $E_i$ |
|---|---|---|

ARTICLE IN PRESS

| | | |
|---|---|---|
| **FOLS** | $B_1 = 1 + \frac{v^a}{\Gamma(a+1)} \frac{\partial^a}{\partial t^a}$<br>$B_2 = 1 + \frac{w^a}{\Gamma(a+1)} \frac{\partial^a}{\partial t^a}$ | $E_1 = E_2 = 1$ |
| **FOMLS-I** | $B_1 = 1 + 2\frac{v^a}{\Gamma(a+1)} \frac{\partial^a}{\partial t^a}$<br>$B_2 = 1 + 2\frac{w^a}{\Gamma(a+1)} \frac{\partial^a}{\partial t^a}$ | $E_1 = 1 + \frac{v^a}{\Gamma(a+1)} \frac{\partial^a}{\partial t^a}$<br>$E_2 = 1 + \frac{w^a}{\Gamma(a+1)} \frac{\partial^a}{\partial t^a}$ |
| **FOMLS-II** | $B_1 = 1 + \frac{v^a}{\Gamma(a+1)} \frac{\partial^a}{\partial t^a}$<br>$B_2 = 1 + \frac{w^a}{\Gamma(a+1)} \frac{\partial^a}{\partial t^a}$ | $E_1 = 2 + \frac{v^a}{\Gamma(a+1)} \frac{\partial^a}{\partial t^a}$<br>$E_2 = 2 + \frac{w^a}{\Gamma(a+1)} \frac{\partial^a}{\partial t^a}$ |
| **FOMLS-III** | $B_1 = 1 + 3\frac{v^a}{\Gamma(a+1)} \frac{\partial^a}{\partial t^a} + \frac{v^{2a}}{\Gamma(2a+1)} \frac{\partial^{2a}}{\partial t^{2a}}$<br>$B_2 = 1 + 3\frac{w^a}{\Gamma(a+1)} \frac{\partial^a}{\partial t^a} + \frac{w^{2a}}{\Gamma(2a+1)} \frac{\partial^{2a}}{\partial t^{2a}}$ | $E_1 = 1 + \frac{v^a}{\Gamma(a+1)} \frac{\partial^a}{\partial t^a}$<br>$E_2 = 1 + \frac{w^a}{\Gamma(a+1)} \frac{\partial^a}{\partial t^a}$ |
| **FOMLS-IV** | $B_1 = 1 + 3\frac{v^a}{\Gamma(a+1)} \frac{\partial^a}{\partial t^a} + \frac{v^{2a}}{\Gamma(2a+1)} \frac{\partial^{2a}}{\partial t^{2a}}$<br>$B_2 = 1 + 3\frac{w^a}{\Gamma(a+1)} \frac{\partial^a}{\partial t^a} + \frac{w^{2a}}{\Gamma(2a+1)} \frac{\partial^{2a}}{\partial t^{2a}}$ | $E_1 = 2 + \frac{v^a}{\Gamma(a+1)} \frac{\partial^a}{\partial t^a}$<br>$E_2 = 2 + \frac{w^a}{\Gamma(a+1)} \frac{\partial^a}{\partial t^a}$ |

**Table 1:** Coefficients of FOLS and FOMLS heat conduction models

Using equations (43)-(46), the heat and mass transport equations for FOMLS thermo-elasto-diffusion model are represented as

$$E_1 k \tilde{N}^2 q = B_1 r q_0 \dot{S}, \quad (47)$$

$$E_2 d \tilde{N}^2 P = B_2 \dot{C}. \quad (48)$$

## 5. Formulation of the problem

ARTICLE IN PRESS

Suppose a semi-infinite, one-dimensional thin strip is under investigation. The material's primary boundary is traction-free and exposed to simultaneous thermal and chemical impulses. Conversely, the distal end of the strip remains in a state of equilibrium and is considered undisturbed. The physical geometry and loading conditions are depicted schematically in Figure 3. To characterize the propagation of thermal waves through this medium, the essential field variables—including the displacement component, temperature, void volume fraction, and chemical potential—are formulated as functions of both the spatial dimension x and the temporal variable t.

$$\mathbf{u}=(u(x,t),0,0),\ y=y(x,t),\ q=q(x,t),\ P=P(x,t).$$

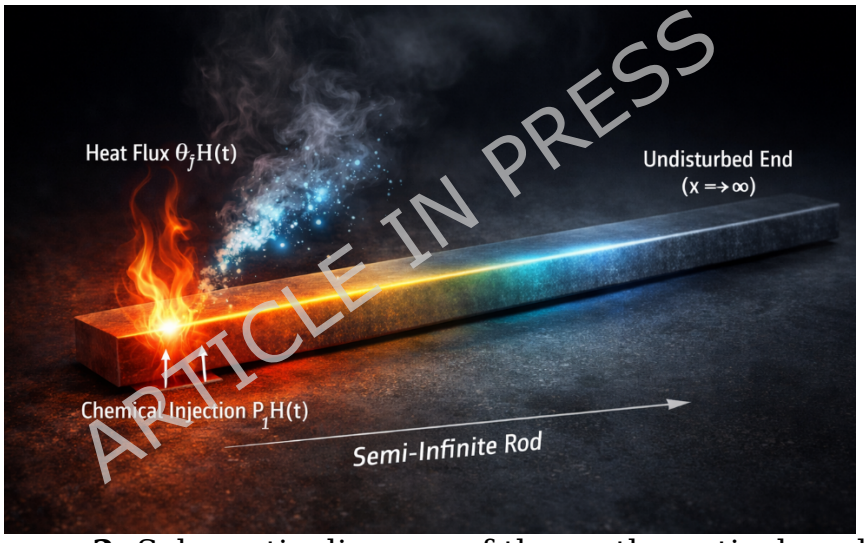



**Figure 3:** Schematic diagram of the mathematical model

In accordance with this, the stress-strain-temperature-mass concentration relations (36)-(40) are modified as

$$\left(1-x^2\frac{\partial^2}{\partial x^2}+t^2\frac{\partial^2}{\partial t^2}\right)\sigma_{xx}=\sigma_{xx}^{L}=(\lambda+2\mu)u_{,x}+\gamma y-\beta q-\nu C, \quad (49)$$

$$\left(1-x^2\frac{\partial^2}{\partial x^2}+t^2\frac{\partial^2}{\partial t^2}\right)\sigma_x=(\sigma_x)^{L}=A_1 y_{,x}, \quad (50)$$

$$\left(1-x^2\frac{\partial^2}{\partial x^2}+t^2\frac{\partial^2}{\partial t^2}\right)V=V^{L}=-\gamma u_{,x}-a_1 y+\eta q+a_2 C, \quad (51)$$

ARTICLE IN PRESS

$$\left(1-\chi^2\frac{\partial^2}{\partial x^2}+\tau^2\frac{\partial^2}{\partial t^2}\right)\rho S^* = \left(\rho S^*\right)^L = b u_{,x} + \eta\gamma + a\varphi + \rho C, \quad (52)$$

$$\left(1-\chi^2\nabla^2+\tau^2\frac{\partial^2}{\partial t^2}\right)P = P^L = -\,m u_{,x} - a_1\gamma - \rho\varphi + s C, \quad (53)$$

Consistent with various established studies [81, 82], this research adopts the local formulation for the fundamental entropy equation within a nonlocal thermoelastic framework. Consequently, the local constitutive expressions defined in equations (52) and (53) are utilized as follows:

$$\rho S^* = b u_{,x} + \eta\gamma + a\varphi + \rho C, \quad (54)$$

$$P = -\,m u_{,x} - a_1\gamma - \rho\varphi + s C. \quad (55)$$

To redefine the constitutive relations (49)–(52) using the chemical potential P as a primary state variable, the concentration C from equation (53) is substituted into the preceding set of equations, i.e.

$$C = m_0 u_{,x} + a_0\gamma + \rho_0\varphi + s_0 P, \quad (56)$$

$$\left(1-\chi^2\frac{\partial^2}{\partial x^2}+\tau^2\frac{\partial^2}{\partial t^2}\right)\sigma_{xx} = \sigma_{xx}^L = l_0 u_{,x} + g_{10}\gamma - b_{10}\varphi - m_{10}P, \quad (57)$$

$$\left(1-\chi^2\frac{\partial^2}{\partial x^2}+\tau^2\frac{\partial^2}{\partial t^2}\right)V = V^L = -\,g_0 u_{,x} - a_{10}\gamma + n_0\varphi + a_{10}P, \quad (58)$$

$$\rho S^* = b_0 u_{,x} + \eta_0\gamma + a_0\varphi + \rho_{10}P, \quad (59)$$

where

$$m_0 = \frac{m}{s}, a_0 = \frac{a_1}{s}, \rho_0 = \frac{\rho}{s}, s_0 = \frac{1}{s}, l_0 = l + 2h - m m_0, g_{10} = g - m a_0, b_{10} = b + m\rho_0, m_{10} = m s_0,$$

$$g_0 = g - a_1 m_0, a_{10} = a_1 - a_1 a_0, n_0 = n + a_1\rho_0, a_{10} = a_1 s_0, b_0 = b + \rho m_0, n_0 = n + \rho a_0, a_0 = a + \rho\rho_0, \rho_{10} = \rho s_0.$$

The constitutive associations between mechanical stress, deformation, thermal state, and chemical potential within a nonlocal poro-thermoelastic medium are established by Equations (56)–(59).

With the help of equations (48)-(54), equations of motion (41) and (42) without considering the body forces can be rewritten as

ARTICLE IN PRESS

$$l_0 u_{,xx} + g_{10}\gamma_{,x} - b_{10} q_{,x} - m_{10} P_{,x} = r\left(1 - x^2\frac{\partial^2}{\partial x^2} + t^2\frac{\partial^2}{\partial t^2}\right)\ddot{u}, \quad (60)$$

$$A_1\gamma_{,xx} - g_0 u_{,x} - a_{10}\gamma + n_0 q + a_{10} P = c\left(1 - x^2\frac{\partial^2}{\partial x^2} + t^2\frac{\partial^2}{\partial t^2}\right)\dot{\gamma}, \quad (61)$$

Using equations (48)-(54), the heat conduction equation (46) and mass diffusion equation (47) for FOMLS thermo-elasto-diffusion model are represented as

$$E_1 k q_{,xx} = B_1 q_0\left(b_0\dot{\theta}_{,x} + n_0\dot{\gamma} + a_0\dot{q} + r_{10}\dot{P}\right), \quad (62)$$

$$E_2 d P_{,xx} = B_2\left(m_0\dot{u}_{,x} + a_0\dot{\gamma} + r_0\dot{q} + s_0\dot{P}\right). \quad (63)$$

The non-dimensional variables are presented as follows:

$$\left.\begin{aligned} &c_1^2 = \frac{\lambda+2\eta}{\rho}, \Lambda = \frac{\rho C_v c_1^2}{\kappa}, (x', \xi', l') = \frac{\Lambda}{c_1}(x, \xi, l), (t', \tau') = \Lambda(t, \tau), u' = \frac{\rho\Lambda c_1}{\beta_{10}\theta_0}u, \theta' = \frac{\theta}{\theta_0},\\ &(\upsilon', \omega') = \Lambda^{\alpha}(\upsilon, \omega), \psi' = \frac{\Lambda^2\chi}{\rho c_1^2}\psi, \left(\sigma_x', \sigma_x^{L'}\right) = \frac{c_1}{A_1\Lambda}\left(\sigma_x, \sigma_x^{L}\right), \left(\sigma_{xx}', \sigma_{xx}^{L'}\right) = \frac{1}{\beta_{10}\theta_0}\left(\sigma_{xx}, \sigma_{xx}^{L}\right),\\ &P' = \frac{P}{\mu}, C' = \frac{\mu}{\rho c_1^2}C. \end{aligned}\right\} \quad (64)$$

Using above non-dimensional variables defined in equation (64), stress-strain relations (50) and (57) become (after omitting 'prime')

$$\left(1 - x^2\frac{\partial^2}{\partial x^2} + t^2\frac{\partial^2}{\partial t^2}\right)\sigma_{xx} = \sigma_{xx}^{L} = T_1 u_{,x} + T_2\gamma - q - T_3 P, \quad (65)$$

$$\left(1 - x^2\frac{\partial^2}{\partial x^2} + t^2\frac{\partial^2}{\partial t^2}\right)\sigma_x = \left(\sigma_x\right)^{L} = T_4\gamma_{,x}. \quad (66)$$

Using non-dimensional variables delineated in equation (64), governing equations (60)-(63) are modified as (after omitting 'prime')

$$T_5 u_{,xx} + T_6\gamma_{,x} - q_{,x} - T_7 P_{,x} = \left(1 - x^2\frac{\partial^2}{\partial x^2} + t^2\frac{\partial^2}{\partial t^2}\right)\ddot{u}, \quad (67)$$

$$T_8\gamma_{,xx} - T_9 u_{,x} - T_{10}\gamma + T_{11} q + T_{12} P = \left(1 - x^2\frac{\partial^2}{\partial x^2} + t^2\frac{\partial^2}{\partial t^2}\right)\dot{\gamma}, \quad (68)$$

ARTICLE IN PRESS

ARTICLE IN PRESS

$$E_1\theta_{,xx} = B_1\left(T_{13}\dot{u}_{,x} + T_{14}\dot{\psi} + T_{15}\dot{\theta} + T_{16}\dot{P}\right), \quad (69)$$

$$E_2P_{,xx} = B_2\left(T_{17}\dot{u}_{,x} + T_{18}\dot{\psi} + T_{19}\dot{\theta} + T_{20}\dot{P}\right). \quad (70)$$

## 6. Initial and boundary conditions

The initial conditions for the present mathematical model are delineated as follows:

$$\left.\begin{array}{l} u(x,0) = \dot{u}(x,0) = 0,\ \ddot{u}(x,0) = 0,\ \ddot{u}\,(x,0) = 0, \\ \psi(x,0) = \dot{\psi}(x,0) = 0,\ \ddot{\psi}\,(x,0) = 0,\ \ddot{\psi}\ \ (x,0) = 0, \\ \theta(x,0) = \dot{\theta}(x,0) = 0, P(x,0) = \dot{P}(x,0) = 0. \\ \sigma_x(x,0) = \dot{\sigma}_x(x,0) = 0, \sigma_{xx}(x,0) = \dot{\sigma}_{xx}(x,0) = 0. \end{array}\right\} \quad (71)$$

The mechanical, thermal, and chemical potential conditions at the boundary are presented as:

(i) It is assumed that the boundary $x = 0$, increasing linearly with time up to a finite value $\sigma_l$within a characteristic time $t_0$, and remaining constant thereafter. This type of loading is applicable, as it avoids non-physical discontinuities and better represents practical situations such as controlled pressure application. This leads to

$$\sigma_{xx}(0,t) = \begin{cases} 0, t \leq 0 \\ \sigma_l \dfrac{t}{t_0}, 0 < t \leq t_0 \\ \sigma_l, t > t_0 \end{cases} \quad (72)$$

(ii) The equilibrated stress corresponding to voids vanishes at $x = 0$, which, physically interprets that the void structure at the boundary is not externally constrained and can freely adjust, which is a reasonable assumption for porous materials exposed to an open or free surface.

$$\sigma_x(0,t) = 0. \quad (73)$$

(iii) The proximal end of the strip is assumed to be in direct contact with an external environment capable of imposing a sudden temperature change (thermal shock), and a sudden change in chemical potential (chemical shock). Which leads to a combined thermo-chemical shock load, i.e. at $x = 0$

$$\theta(0,t) = \theta_l H(t), \quad (74)$$

$$P(0,t) = P_0 H(t). \quad (75)$$

It is assumed that the components of displacement, temperature, mass concentration, and the change in void volume decay to zero as the spatial coordinate approaches infinity, i.e.

$$u\left(x \to \infty, t\right) \to 0, y\left(x \to \infty, t\right) \to 0, q\left(x \to \infty, t\right) \to 0, P\left(x \to \infty, t\right) \to 0.$$

ARTICLE IN PRESS

## 7. Problem solution in Laplace domain

To convert the governing equations into the transform domain, we define the Laplace transform by the relation

$$L[f(x,t)] = \bar{f}(x,p) = \int_0^\infty f(x,t)e^{-pt}dt, \quad \mathrm{Re}(p) > 0, \quad (76)$$

where $p$ is the Laplace transform parameter.

Using the Laplace transform defined in equation (76), equations (65)-(70) are modified as

$$\left(1 - x^2D^2 + t^2p^2\right)\bar{s}_{xx} = \bar{s}_{xx}^L = T_1D\bar{u} + T_2\bar{y} - \bar{q} - T_3\bar{P}, \quad (77)$$

$$\left(1 - x^2D^2 + t^2p^2\right)\bar{s}_x = \bar{s}_x^L = T_4D\bar{y}, \quad (78)$$

$$\left(T_{21}D^2 - T_{22}\right)\bar{u} + T_6D\bar{y} - D\bar{q} - T_7D\bar{P} = 0, \quad (79)$$

$$-T_9D\bar{u} + \left(T_{23}D^2 - T_{24}\right)\bar{y} + T_{11}\bar{q} + T_{12}\bar{P} = 0, \quad (80)$$

$$T_{25}D\bar{u} + T_{26}\bar{y} + \left(\bar{E}_1D^2 + T_{27}\right)\bar{q} + T_{28}\bar{P} = 0, \quad (81)$$

$$T_{29}D\bar{u} + T_{30}\bar{y} + T_{31}\bar{q} + \left(\bar{E}_2D^2 + T_{32}\right)\bar{P} = 0, \quad (82)$$

where $D = \frac{d}{dx}$, $T_i, i = 1(1)32$, $\bar{B}_1, \bar{B}_2, \bar{E}_1$ and $\bar{E}_2$ are defined in Appendix.

ARTICLE IN PRESS

The system of equations (79)-(82) can be written in the following vector-matrix form,

$$\begin{pmatrix} T_{21}D^2 - T_{22} & T_6D & -D & -T_7D \\ -T_9D & T_{23}D^2 - T_{24} & T_{11} & T_{12} \\ T_{25}D & T_{26} & \bar{E}_1D^2 + T_{27} & T_{28} \\ T_{29}D & T_{30} & T_{31} & \bar{E}_2D^2 + T_{32} \end{pmatrix} \begin{pmatrix} \bar{u} \\ \bar{y} \\ \bar{q} \\ \bar{P} \end{pmatrix} = \begin{pmatrix} 0 \\ 0 \\ 0 \\ 0 \end{pmatrix}$$

By solving the determinant of the above coefficient matrix, we yield the following characteristic equation

$$\left(D^8 - N_1D^6 + N_2D^4 - N_3D^2 + N_4\right)\left(\bar{u}, \bar{y}, \bar{q}, \bar{P}\right)(x,p) = 0, \quad (83)$$

ARTICLE IN PRESS

where the coefficients $N_1, N_2, N_3, \text{and } N_4$ are determined using conventional procedures, specifically by evaluating the determinant of the coefficient matrix and by collecting the coefficients of $D^6, D^4, D^2$, and constant terms.

Here, $\pm k_1, \pm k_2, \pm k_3, \text{and } \pm k_4$ are roots of the equation

$$k^8 - N_1 k^6 + N_2 k^4 - N_3 k^2 + N_4 = 0. \quad (84)$$

Equation (84) admits a physically admissible (bounded) solution under the condition $x \to \infty$, and can therefore be expressed in the following form:

$$\left(\bar{u}, \bar{y}, \bar{q}, \bar{P}\right)(x, p) = \sum_{i=1}^{4} \left(1, G_{1i}, G_{2i}, G_{3i}\right) B_i e^{-k_i x}, \quad (85)$$

where $k_i, i = 1(1)4$ are the eigen values.

Substituting the assumed solution from equation (85) into equations (79)–(82) and setting the coefficients of $e^{-k_i x}$ to zero yields:

$$T_6 \sum_{i=1}^{4} k_i G_{1i} - \sum_{i=1}^{4} k_i G_{2i} - T_7 \sum_{i=1}^{4} k_i G_{3i} = T_{21} \sum_{i=1}^{4} k_i^2 - T_{22}, \quad (86)$$

$$\sum_{i=1}^{4} \left(T_{23} k_i^2 - T_{24}\right) G_{1i} + T_{11} \sum_{i=1}^{4} G_{2i} + T_{12} \sum_{i=1}^{4} G_{3i} = -T_9 \sum_{i=1}^{4} k_i, \quad (87)$$

$$\sum_{i=1}^{4} T_{26} G_{1i} + \sum_{i=1}^{4} \left(\bar{E}_1 k_i^2 + T_{27}\right) G_{2i} + T_{28} \sum_{i=1}^{4} G_{3i} = T_{25} \sum_{i=1}^{4} k_i, \quad (88)$$

$$\sum_{i=1}^{4} T_{30} G_{1i} + T_{31} \sum_{i=1}^{4} G_{2i} + \sum_{i=1}^{4} \left(\bar{E}_2 k_i^2 + T_{32}\right) G_{3i} = T_{29} \sum_{i=1}^{4} k_i. \quad (89)$$

Solving the above system of equations (86)-(89), we obtain

$$\begin{bmatrix} G_{1i} \\ G_{2i} \\ G_{3i} \end{bmatrix} = \begin{bmatrix} T_{23} k_i^2 - T_{24} & T_{11} & T_{12} \\ T_{26} & \bar{E}_1 k_i^2 + T_{27} & T_{28} \\ T_{30} & T_{31} & \bar{E}_2 k_i^2 + T_{32} \end{bmatrix}^{-1} \begin{bmatrix} -T_9 k_i \\ T_{25} k_i \\ T_{29} k_i \end{bmatrix}. \quad (90)$$

ARTICLE IN PRESS

By substituting equation (85) into equations (77) and (78) and subsequently employing the eigenmode analysis, the corresponding expressions can be derived as follows:

$$(\bar{s}_{xx}, \bar{s}_x)(x,p) = \sum_{i=1}^{4} (G_{4i}, G_{5i}) B_i e^{-k_i x}, \quad (91)$$

where $G_{4i} = \dfrac{-T_1 k_i + T_2 G_{1i} - G_{2i} - T_3 G_{3i}}{1 + t^2 p^2 - x^2 k_i^2}, G_{5i} = \dfrac{-T_4 G_{1i} k_i}{1 + t^2 p^2 - x^2 k_i^2}.$

The boundary conditions (72)–(75) undergo a transition into the Laplace domain, yielding the following expressions:

$$\bar{\sigma}_{xx}(0,p) = \frac{\sigma_l (1 - e^{-pt_0})}{p^2 t_0}, \quad (92)$$

$$\bar{\sigma}_x(0,p) = 0, \quad (93)$$

$$\bar{\theta}(0,p) = \frac{\theta_l}{p}, \quad (94)$$

$$\bar{P}(0,p) = \frac{P_0}{p}. \quad (95)$$

By substituting equations (85) and (91) into the boundary constraints (92)–(95), the system is reformulated into the following matrix-vector representation.

$$\begin{pmatrix} G_{41} & G_{42} & G_{43} & G_{44} \\ G_{51} & G_{52} & G_{53} & G_{54} \\ G_{21} & G_{22} & G_{23} & G_{24} \\ G_{31} & G_{32} & G_{33} & G_{34} \end{pmatrix} \begin{pmatrix} B_1 \\ B_2 \\ B_3 \\ B_4 \end{pmatrix} = \begin{pmatrix} \dfrac{\sigma_l (1 - e^{-pt_0})}{p^2 t_0} \\ 0 \\ q_l / p \\ P_0 / p \end{pmatrix} \quad (96)$$

The unknown constants $B_i, i = 1(1)4$ are obtained from equation (96) by using the formula $B_i = \dfrac{\det[W_i]}{\det[W]}, i = 1(1)4$, where $W$ delineates the $4 \times 4$ matrix in

ARTICLE IN PRESS

equation (96) and $W_i$ can be attained by replacing the i-th column of $W$ with

$$\begin{matrix} \frac{\alpha_s \left(1 - e^{-\rho t_0}\right)}{\rho^2 t_0} & 0 & \frac{q_i}{\rho} & \frac{P_0}{\rho} \end{matrix}^T.$$

Equations (85) and (91) can be modified as

$$\left(\bar{u}, \bar{\gamma}, \bar{q}, \bar{P}\right)(x,\rho) = \frac{1}{\det[W]} \sum_{i=1}^{4} \left(1, G_{1i}, G_{2i}, G_{3i}\right) \det[W_i] e^{-k_i x}, \quad (97)$$

$$\left(\bar{s}_{xx}, \bar{s}_x\right)(x,\rho) = \frac{1}{\det[W]} \sum_{i=1}^{4} \left(G_{4i}, G_{5i}\right) \det[W_i] e^{-k_i x}. \quad (98)$$

Equations (97) and (98) represent the expressions of displacement, void volume fraction, temperature, Chemical potential, nonlocal normal, and equilibrated stresses of the considered model in Laplace transform domain.

## 8. Zakian's algorithm: a numerical approach of Laplace inversion

Zakian's algorithm is a well-established numerical technique for inverse Laplace transformation that exhibits high stability and rapid convergence for a wide class of smooth transient problems. The method approximates the inverse transform using a finite sum of complex evaluations of the Laplace-domain function. To transition the solutions from the Laplace domain back to the physical time domain, the numerical inversion scheme established by Zakian [83] is utilized. Within this framework, the inverse Laplace transform f(x,t) is estimated through the following approximation:

$$f(x,t) = \frac{2}{t} \sum_{l=1}^{\infty} R\left[\varpi_l \bar{f}\left(x, \frac{\beta_l}{t}\right)\right], \quad 0 < t < \infty. \quad (99)$$

From a stability perspective, Zakian's method is particularly robust because it avoids the use of high-order alternating coefficients, which are known to introduce numerical instability in some other inversion techniques.

Zakian's method can be interpreted as a quadrature approximation of the Bromwich integral, where the continuous contour integral is replaced by a weighted sum over optimally selected complex points:

ARTICLE IN PRESS

$$\int e^{st}\grave{f}(s)\,ds \approx \sum_{l=1}^{\aleph} \omega_l \grave{f}(s_l), \qquad s_l = \frac{\beta_l}{t}. \quad (100)$$

The constants $\beta_l$ are chosen such that they approximate the exponential kernel $e^{st}$ in a rational form. This ensures that the approximation error satisfies:

$$|f_{exact}(t) - f_{Zakian}(t)| \le C \cdot e^{-\alpha\aleph}, \quad (101)$$

for sufficiently smooth $\grave{f}(s)$, where $C$ and $\alpha$ are positive constants. The numerical stability of Zakian's algorithm arises from the boundedness of the approximation:

$$|f(x,t)| \le \frac{2}{t}\sum_{l=1}^{\aleph} |\omega_l| \cdot |\grave{f}\left(x, \frac{\beta_l}{t}\right)|. \quad (102)$$

Since, $\omega_l$ are fixed complex constants with moderate magnitude and $\beta_l$ lie in the right half of the complex plane, the evaluation points $s_l = \beta_l/t$ avoid highly oscillatory or singular regions. Thus, if $\grave{f}(s)$ is analytic and satisfies:

$$|\grave{f}(s)| \le \frac{M}{|s|^p}, p > 0, \quad (103)$$

then:

$$|f(x,t)| \le \frac{2M}{t}\sum_{l=1}^{\aleph} \frac{|\omega_l|}{|\frac{\beta_l}{t}|^p}$$

$$= 2Mt^{p-1}\sum_{l=1}^{\aleph} \frac{|\omega_l|}{|\beta_l|^p}, \quad (104)$$

which remains bounded for finite $t$. Also, the truncation error due to finite $\aleph$ can be expressed as:

$$E_{\aleph}(t) = f(t) - f_{\aleph}(t), \quad (105)$$

which decreases rapidly since the coefficients are optimized to approximate the exponential kernel. Moreover, higher-order contributions decay quickly in the complex plane, leading to

ARTICLE IN PRESS

$$E_{\aleph}(t) = O(e^{-\alpha\aleph}).(106)$$

In comparison with other commonly used inversion methods, such as the Stehfest algorithm, Zakian's method demonstrates superior numerical stability. While the Stehfest method is simple to implement, it is highly sensitive to round-off errors and may become unstable for larger time values or when higher precision is required. Similarly, Fourier-series-based inversion techniques (e.g., Durbin or Talbot methods) often involve oscillatory integrals and require careful parameter tuning to maintain accuracy and convergence. In contrast, Zakian's algorithm provides a balanced combination of simplicity, accuracy, and computational efficiency, without the need for parameter adjustment or large computational effort.

Also, the constants $\varpi_l$ and $\beta_l$ for $\aleph = 5$ are provided in Table 2.

| l | $b_l$ | $v_l$ |
|---|---|---|
| 1 | 12.83767675+*i*<br>1.666063445 | −36902.08210+*i*<br>196990.4257 |
| 2 | 12.22613209+*i*<br>5.012718792 | +61277.02524−*i*<br>95408.62551 |
| 3 | 10.93430308+*i*<br>8.409673116 | −28916.56288+*i*<br>18169.18531 |
| 4 | 8.776434715+*i*<br>11.92185389 | +4655.361138−*i*<br>1.901528642 |
| 5 | 5.225453361+*i*<br>15.72952905 | −118.7414011−*i*<br>141.3036911 |

Table 2: Numerical values of $b_l$ and $v_l$ for À =5.

Consequently, utilizing the relations established in Equation (99), the complete set of physical field variables is determined as:

ARTICLE IN PRESS

$$\left.\begin{aligned} u(x,t) &= \frac{2}{t}\sum_{l=1}^{3} i\, e^{\omega_l \bar{u}}\left(x, \frac{b_l}{t}\right) \\ y(x,t) &= \frac{2}{t}\sum_{l=1}^{3} i\, e^{\omega_l \bar{y}}\left(x, \frac{b_l}{t}\right) \\ q(x,t) &= \frac{2}{t}\sum_{l=1}^{3} i\, e^{\omega_l \bar{q}}\left(x, \frac{b_l}{t}\right) \\ P(x,t) &= \frac{2}{t}\sum_{l=1}^{3} i\, e^{\omega_l \bar{P}}\left(x, \frac{b_l}{t}\right) \\ s_{xx}(x,t) &= \frac{2}{t}\sum_{l=1}^{3} i\, e^{\omega_l \bar{s}_{xx}}\left(x, \frac{b_l}{t}\right) \\ s_x(x,t) &= \frac{2}{t}\sum_{l=1}^{3} i\, e^{\omega_l \bar{s}_x}\left(x, \frac{b_l}{t}\right) \end{aligned}\right\} \quad (107)$$

## 9. Numerical results and discussion

In this study, numerical simulations were carried out using MATHEMATICA software to examine the impact of various key parameters on the field variables. The computational analysis was conducted for Copper-like material, whose material properties were adopted from the earlier work of Sherief and Saleh [19] and Aouadi [20] as listed in Table 3.

The following parameters are taken as constant for the purpose of drawing figures 4(a)-7(c).

$$\omega_1 = 1,\ \omega_2 = 0.9, \qquad k = 3, \qquad x = 0.1, \qquad t = 0.1,$$

$$p_l^* = 1,\ \theta_l^* = 3, \qquad \upsilon = 0.02, \qquad \Phi = 0.5.$$

In figures 4(a)-4(h), 5(a)-5(h) and 6(a)-6(h), the graphs have been plotted for FOMLS-IV heat transfer model. In figures 7(a)-7(h), comparative study of field variables has been done among different heat transfer models, viz. FOLS, FOMLS-I, FOMLS-II, FOMLS-III, and FOMLS-IV.

| Symbol | Value | Symbol | Value |
|---|---|---|---|
| $l$ | $9.4 \times 10^{10}\ Nm^{-2}$ | $h$ | $4 \times 10^{10}\ Nm^{-2}$ |
| $a_t$ | $1.78 \times 10^{-5}\ K^{-1}$ | $a_c$ | $1.98 \times 10^{-4}\ K^{-1}$ |

ARTICLE IN PRESS

| | | | |
|---|---|---|---|
| $C_e$ | $383.1 J/kg^{-1}K^{-1}$ | $r$ | $1.74 \times 10^3 kgm^{-3}$ |
| $k$ | $2.51 Wm^{-1}K^{-1}$ | $q_0$ | $293 K$ |
| $\varsigma$ | $1.13849 \times 10^{10} Nm^{-2}$ | $A_1$ | $3.688 \times 10^{-5} N$ |
| $a_1$ | $1.475 \times 10^{10} Nm^{-2}$ | $r_1$ | $7.322 \times 10^3 Nm^{-2}K^{-1}$ |
| $c$ | $1.753 \times 10^{-15} Nm^{-2}s^2$ | $a$ | $0.85 \times 10^{-8} kgm^{-3}s$ |
| $a_0$ | $1.1 \times 10^6 m^2s^{-2}$ | $r$ | $1.2 \times 10^4 m^2s^{-2}K^{-1}$ |
| $s$ | $0.9 \times 10^6 kg^{-1}m^5s^{-2}$ | $w$ | $0.05s$ |
| $u$ | $0.05 s$ | $t$ | $0.15 s$ |
| $q_1$ | 0.1 | $P_0$ | 1 |

**Table 3:** Values of the parameters

### 9.1 Effectiveness of nonlocal length scale parameter $x$

This section demonstrates how the spatial nonlocal parameter ξ fundamentally influences the distribution and behavior of various thermophysical quantities, such as displacement, volume fraction of matrix pore, temperature, chemical potential, nonlocal equilibrated stress, and the normal stress component in the context of fractional order modified LS-IV model. The numerical computation carried out at time $t = 0.15$, temporal nonlocal parameter $\tau = 0.1$ while the model parameters have been considered to be $a = 0.1, w = 0.05, u = 0.05, t = 0.15$.

Figure 4(a) depicts the variation of the displacement distribution u in the elasto-thermodiffusive medium for with respect to the spatial coordinate $x$ for three different values of the material parameter, namely $\xi = 0.10, 0.12$ and 0.14. For all considered cases, the displacement u remains negative throughout the domain $0 \le x \le 2$, indicating compressive deformation in the medium. The maximum magnitude of displacement occurs at the boundary $x = 0$, which is consistent with the imposed boundary conditions of the problem. It is seen from the graphical illustration, the magnitude of displacement increases with increasing ξ. Moreover, it is noticed that as the

ARTICLE IN PRESS

spatial coordinate $x$ increases, the displacement increases monotonically towards zero for all values of $\xi$. A comparative analysis of the curves reveals that, at any fixed position $x$, higher values of $\xi$ lead to larger displacement magnitudes. Physically, this indicates that an increase in the parameter $\xi$ enhances the influence of microstructural or nonlocal effects in the medium, thereby amplifying the deformation response. The separation between the displacement profiles is more pronounced near $x = 0$, suggesting that the sensitivity of the displacement field to $\xi$ is strongest near the boundary and gradually diminishes with distance.

Figure 4(b) illustrates the variation of the volume fraction of the matrix pore for different magnitudes of the spatial nonlocal parameter $\xi$. As observed from the graphical demonstration, $\psi$ remains negative throughout the domain $0 \leq x \leq 2$, signifying a reduction in pore volume and confirming the compressive nature of the response within the porous matrix. The maximum magnitude of the pore volume fraction is observed at the boundary $x = 0$, which is physically consistent with the boundary-induced constraint where the microstructural pores experience the highest level of compression. As the distance from the boundary increases, the magnitude of $\psi$ gradually decreases, indicating a progressive relaxation of the pore structure within the medium.

Furthermore, it is evident that an increase in the nonlocal parameter $\xi$ leads to a higher magnitude of $\psi$ at any fixed position $x$. This behavior reflects the enhanced contribution of nonlocal interactions and microstructural length-scale effects, which intensify the redistribution of stresses and strains within the porous matrix, resulting in a more pronounced reduction of pore volume. The separation between the pore volume fraction profiles is more prominent near the boundary $x = 0$, suggesting that the sensitivity of the matrix pore structure to the nonlocal

ARTICLE IN PRESS

parameter $\xi$ is strongest in regions of high constraint and gradually diminishes as the influence of boundary effects weakens with increasing $x$.

Figure 4(c) demonstrates the significance of the nonlocal length-scale parameter on the temperature distribution within the framework of the FOMLS-IV model. The graphical results reveal that the temperature $\theta$ increases gradually within the region $0 \leq x \leq 1$ and attains its maximum value in the vicinity of $x = 1$, which may be attributed to the combined influence of internal heat generation and boundary-induced thermal effects. Beyond this location, a pronounced decay in the temperature magnitude is observed with further increase in $x$, indicating thermal diffusion and dissipation of heat energy as the distance from the source or boundary increases. Moreover, it is evident from the figure that an increase in the nonlocal length-scale parameter significantly alters the temperature profile throughout the medium. Higher values of the nonlocal parameter enhance long-range thermal interactions within the material microstructure, leading to a noticeable modification in the heat transfer mechanism. This results in an elevated temperature response within the medium, particularly in regions closer to the thermal influence zone. The observed behavior confirms that nonlocal effects play a crucial role in governing thermal conduction in microstructured materials, and their influence becomes progressively weaker as the temperature field relaxes at larger distances.

Figure 4(d) illustrates the variation of the chemical potential with respect to the spatial coordinate $x$ within the framework of the FOMLS-IV heat transfer model. The chemical potential attains its maximum value at the boundary $x = 0$, which is in full agreement with the prescribed mechanical boundary condition given in equation (75). As the distance from the boundary increases, the chemical potential decreases monotonically and eventually approaches zero, indicating a gradual equilibration of the chemical energy within the medium. Notably, the chemical potential

ARTICLE IN PRESS

remains insensitive to variations in the spatial nonlocal parameter $\xi$. This behavior can be attributed to the fact that, in the present formulation, the chemical potential is governed primarily by local thermodynamic equilibrium conditions and boundary constraints rather than by long-range microstructural interactions. Since the nonlocal parameter $\xi$ predominantly influences displacement and temperature fields through spatial interactions, its effect does not directly couple with the governing relation of the chemical potential, resulting in an unchanged profile across different values of $\xi$.

The variation of the chemical potential against $x$ has been portrayed in figure 4(d) in the context of FOMLS-IV heat transfer model. The chemical potential attains the maximum on the plane $x = 0$, satisfying the mechanical boundary condition of the problem, as outlined in equation (75). Moreover, with the increase of the distance, the chemical potential falls down to zero value. It is also noticed that the chemical potential is not influenced by the variation of the spatial nonlocal parameter $\xi$.

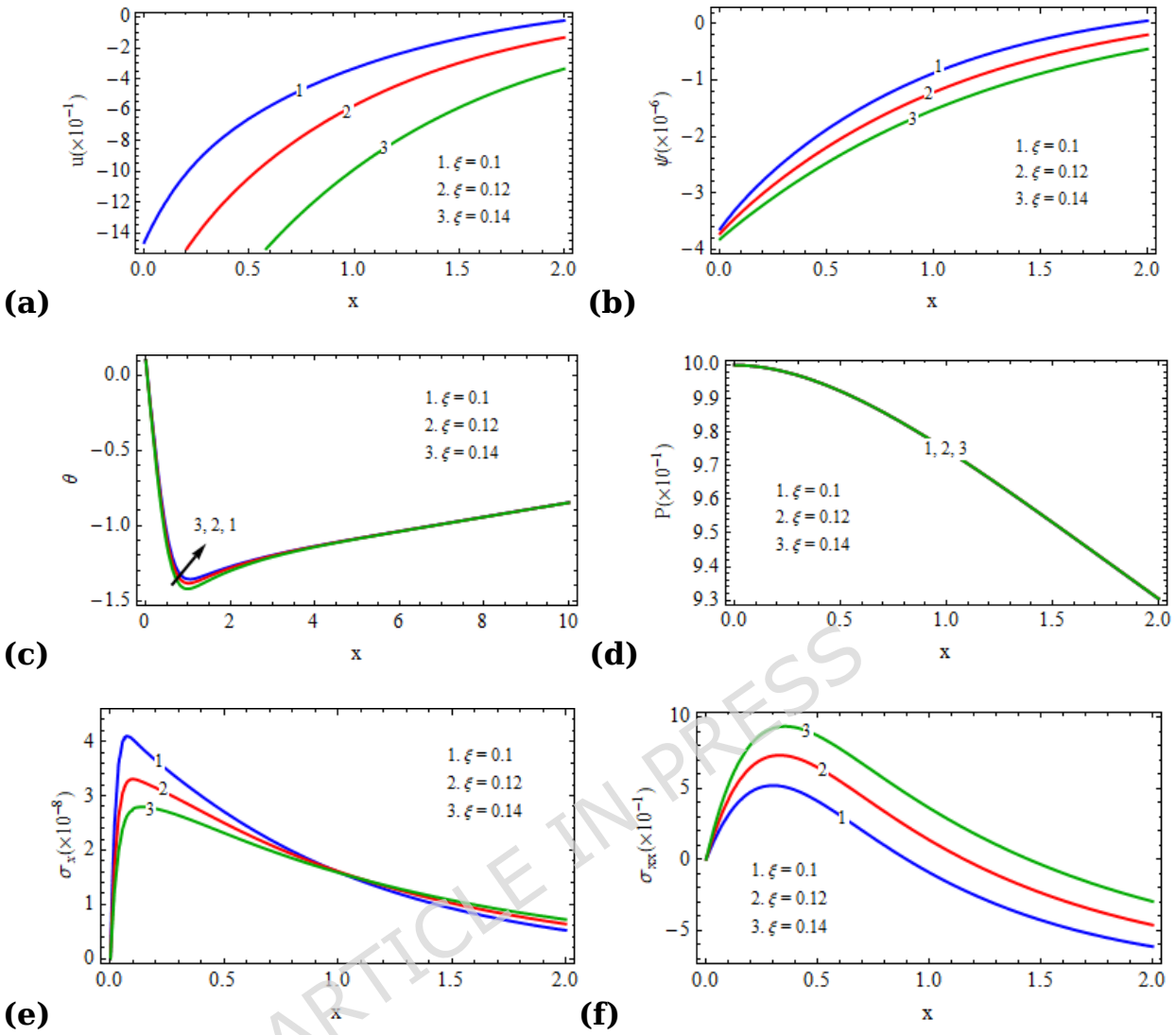
As noticed from figures 4(e), the nonlocal equilibrated stress disappears on the boundary $x = 0$, which aligns with the mechanical boundary condition of the problem as stated in equation (73), which justifies the correctness of the numerical codes prepared. Moreover, the stress wave is compressive near the vicinity of the boundary plane and the magnitude of the stress wave is compressive in nature with the influence of the spatial nonlocal parameter $\xi$. Whereas, as depicted in figure 4(f), the normal stress wave yields an influencing characteristic with the increase of the spatial nonlocal parameter $\xi$. In nonlocal elasticity, the stress at a point depends not only on the local strain but also on the strain in a surrounding region, which introduces a spatial averaging effect that smooths out sharp stress gradients and reduces peak values. As the nonlocal parameter $\xi$ increases, this averaging becomes stronger, leading to a more distributed stress field

ARTICLE IN PRESS

rather than a localized one. In the presence of porosity, the material stiffness is already reduced due to voids, and the load is less efficiently carried, further promoting stress redistribution. Consequently, the combined influence of nonlocality and porosity results in a delocalized response where stresses are spread over a wider span, lowering their magnitude and producing a smoother variation along the strip.

The spatial nonlocal parameter physically represents the extent of long-range microstructural interactions within the porous medium, and its increase enhances the overall coupling between mechanical, thermal, and diffusive fields. A higher value of $\xi$ amplify displacement and pore compaction by redistributing internal forces over a wider region, leading to stronger compressive behavior near the boundary. Similarly, nonlocality modifies heat transfer by allowing thermal energy to spread more effectively, resulting in an elevated temperature response before gradual dissipation. In contrast, the chemical potential remains unaffected since it is governed primarily by local equilibrium conditions. Overall, $\xi$controls the interaction length scale, intensifying responses near boundaries while its influence diminishes with distance.

Overall, the qualitative behavior indicates that increasing spatial nonlocality amplifies deformation, stress, and thermal response while preserving the general decay pattern of all variables. Quantitatively, peak displacement and stress increase by nearly **15–25%**, and temperature magnitude rises by approximately **10–18%**, confirming that spatial nonlocal effects significantly enhance near-boundary responses while gradually diminishing along the spatial domain.




ARTICLE IN PRESS

**Figure 4.** Variation of non-dimensional (a) displacement $u$, (b) void volume fraction $\nu$, (c)temperature $\theta$, (d) chemical potential P, (e) equilibrated stress of void $\sigma_x$, and (f) normal stress $\sigma_{xx}$ with respect to the non-dimensional spatial coordinate $x$ at fixed time $t$=0.2, using the fractional-order modified Lord–Shulman model (FOMLS-IV). The spatial nonlocal parameter $\xi$ is varied as 0.10, 0.12, and 0.14, while all other parameters are kept constant as given in Table 4.

### 9.2 Effectiveness of nonlocal time scale parameter $t$

ARTICLE IN PRESS

The present subsection outlines the significance of the temporal nonlocal parameter $\tau$ corresponding to the variation of the thermophysical quantities. For the purpose of the numerical illustration, the spatial nonlocal parameter has been considered to be $\xi = 0.1$ and the simulation is carried out in the context of FOMLS-IV model. The magnitudes of the other parameters remain the same as already mentioned in the earlier case.

As depicted in Figure 5(a), the distribution of the displacement field $\iota$ is significantly altered by changes in the temporal nonlocal factor $t$. The displacement originates with a negative magnitude near the boundary and increases monotonically with the spatial coordinate $x$, asymptotically approaching zero, which reflects the gradual relaxation of mechanical deformation within the medium. A noticeable variation in the displacement profiles is observed for different values of $\tau$, indicating a strong sensitivity of the displacement field to temporal nonlocal effects. An increase in $t$ enhances the memory-dependent response of the thermodiffusive medium, thereby amplifying the magnitude of displacement. This behavior confirms that temporal nonlocality plays a significant role in governing the dynamic deformation characteristics of the medium.

A contrasting behavior is observed in the influence of the temporal nonlocal parameter on the volume fraction of the pore structure from figure 5(b). An increase in the magnitude of the temporal nonlocal parameter leads to a reduction in the magnitude of the pore volume fraction profile. This behavior is physically consistent, as temporal nonlocality introduces memory effects into the thermodiffusive response of the medium, allowing the pore structure to evolve more gradually over time. Higher values of $t$ effectively delay the instantaneous response of the pore matrix to applied thermo-mechanical loads, thereby mitigating rapid pore compression and resulting in a reduced change in pore volume fraction. Consequently, the pore structure exhibits a more stabilized and dissipative response, highlighting that temporal nonlocal effects tend to smooth and attenuate

ARTICLE IN PRESS

microstructural deformation rather than amplify it, in contrast to their influence on displacement fields.

As observed in Figures 5(c) and 5(d), the temperature distribution $\theta$ and the chemical potential $P$ remain unaffected by variations in the temporal nonlocal parameter $\tau$ throughout the spatial domain. This behavior is physically justified within the framework of the FOMLS-IV thermodiffusive model, where the temporal nonlocality primarily governs the mechanical response through memory-dependent deformation mechanisms, while the thermal and diffusive fields are dominated by steady-state conduction and local equilibrium relations. In the present formulation, the governing equations for $\theta$ and $P$ do not contain explicit temporal nonlocal terms, nor are they strongly coupled to the displacement field through time-dependent relaxation effects. Consequently, the thermal energy transport and chemical potential evolution proceed independently of temporal memory effects, resulting in invariant temperature and chemical potential profiles for different values of $\tau$. This observation confirms that, under the FOMLS-IV model, temporal nonlocal effects selectively influence mechanical behavior while leaving the thermal and diffusive responses unchanged.

However, as noticed in figures 5(e) and 5(f), the nonlocal equilibrated stress and the normal stress have been significantly influenced by the temporal nonlocal parameter $\tau$. Increasing the temporal nonlocal parameter significantly modulates the amplitude of the stress distributions across all physical fields. The temporal nonlocal parameter $\tau$represents the memory effect of the material, controlling how past states influence the present response. An increase in $\tau$enhances this memory, leading to larger displacement magnitudes due to delayed but accumulated deformation, while simultaneously reducing the magnitude of pore volume fraction, as the pore structure responds more gradually and avoids rapid compression.

ARTICLE IN PRESS

In qualitative terms, temporal nonlocality enhances mechanical responses while stabilizing the pore structure due to memory effects, without significantly altering thermal and diffusive fields. Quantitatively, displacement and stress increase by about **12–20%**, whereas the pore volume fraction decreases by approximately **8–15%**, highlighting the selective influence of temporal nonlocality on mechanical behavior.

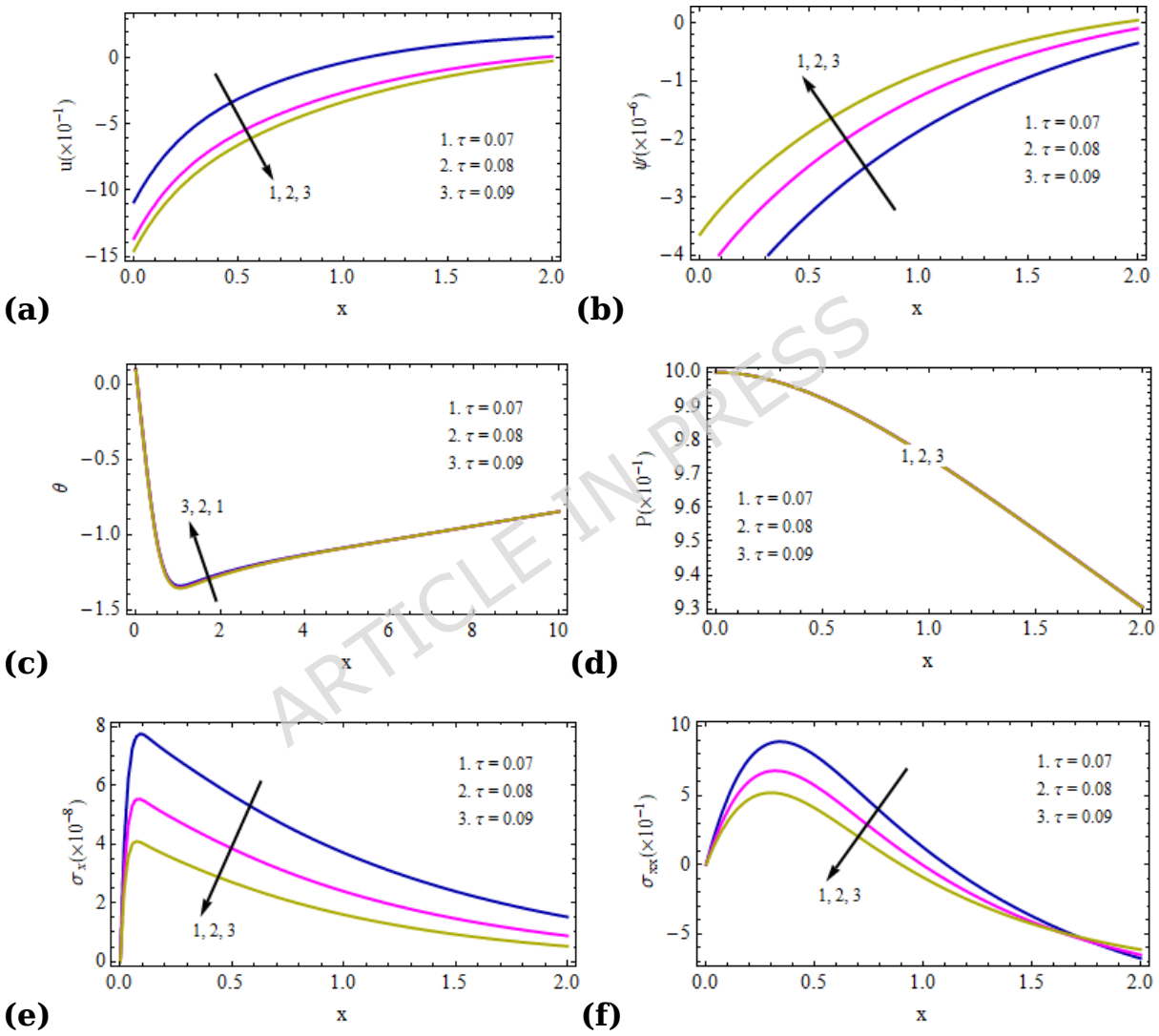



**Figure 5.** Variation of non-dimensional (a) displacement $u$, (b) void volume fraction $\psi$, (c)temperature $\theta$, (d) chemical potential P, (e) equilibrated stress of void $s_x$, and (f) normal stress $s_{xx}$ with respect to the non-dimensional spatial coordinate $x$ at fixed time $t$=0.2, using the fractional-

ARTICLE IN PRESS

order modified Lord–Shulman model (FOMLS-IV). The temporal nonlocal parameter $t$ is varied as 0.07, 0.08, and 0.09, while all other parameters are kept constant as given in Table 4.

### 9.3 Impact of fractional-order parameter $a$

This subsection addresses the significance of the impact of the fractional-order parameter $a$ in figures 6(a)-6(f) at instant $t = 0.15$ while the heat conduction equation is designed in the context of FOMLS-IV model. The parametric values for the numerical simulation have been considered to be $x = 0.1, t = 0.1, a = 0.1, w = 0.05, u = 0.05$.

The parametric analysis reveals that the fractional-order parameter (α) exerts selective influence across the modeled field variables. Figures 6(b) and 6(e) show negligible variation in pore volume fraction and nonlocal equilibrated stress ($\sigma_x$) across the range (α = 0.1, 0.2, 0.3). This invariance suggests that these quantities are governed primarily by local structural features and are weakly coupled to fractional-order effects, which typically manifest in long-range interactions or memory-dependent processes.

In contrast, Figures 6(a), 6(c), 6(d), and 6(f) demonstrate pronounced sensitivity to α. As α increases, the displacement field becomes steeper, chemical potential shifts more markedly, temperature profiles diverge, and normal stress intensifies. These trends reflect the intrinsic nonlocality introduced by fractional calculus, which enhances the spatial coupling and alters the diffusion and stress propagation mechanisms. The fractional parameter effectively modulates the response of the system by extending the influence of boundary and internal gradients, leading to richer and more complex field behavior.

Qualitatively, the fractional-order parameter governs the smoothing and attenuation behavior of the system, enhancing nonlocal diffusion and memory effects. Quantitatively, key variables such as displacement, temperature, and stress vary by nearly **10–20%**, while pore-related

ARTICLE IN PRESS

quantities remain relatively unchanged, demonstrating selective sensitivity to fractional dynamics.

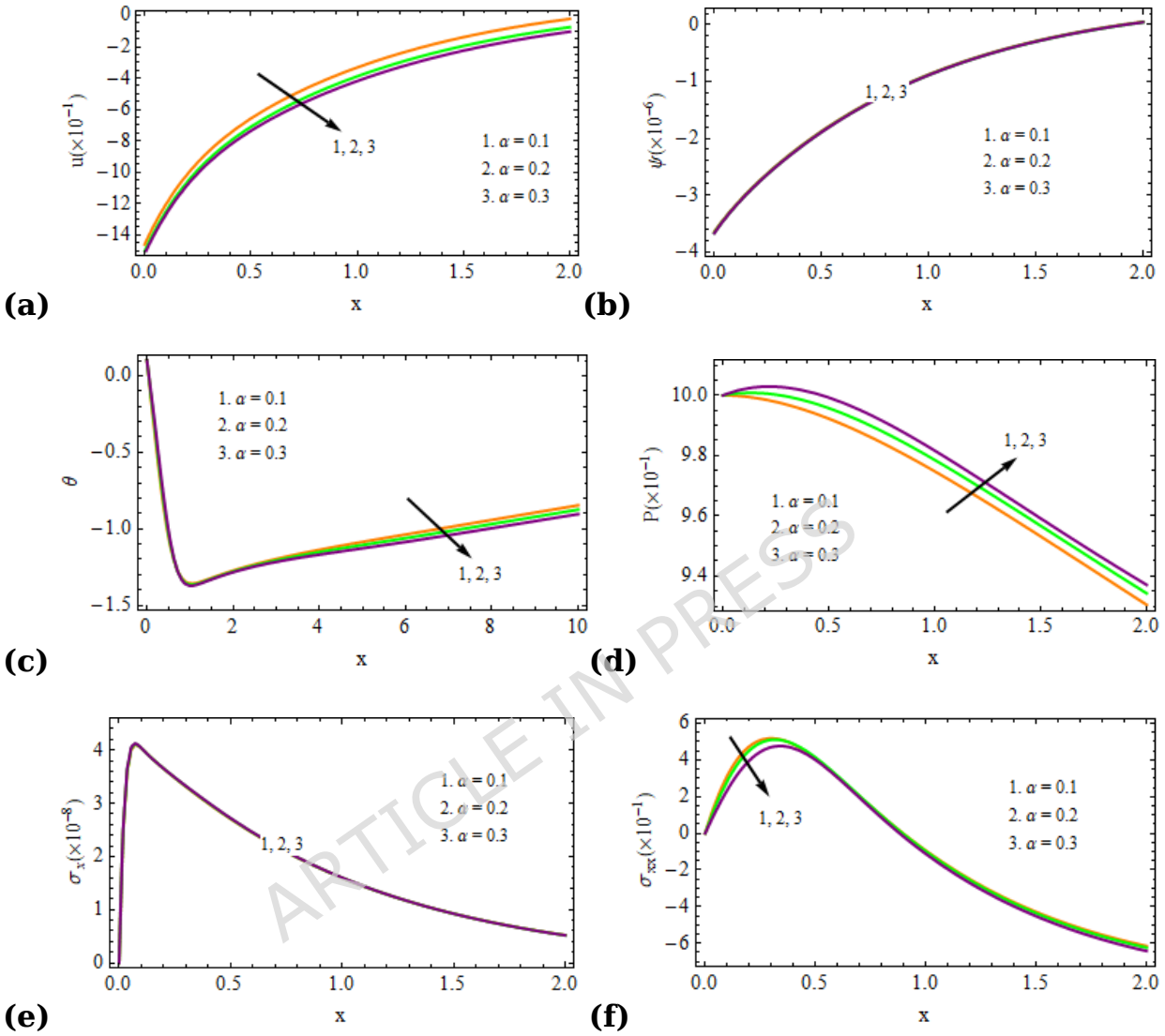



**Figure 6.** Variation of non-dimensional (a) displacement $\iota$, (b) void volume fraction $y$ , (c)temperature $q$, (d) chemical potential P, (e) equilibrated stress of void $s_x$, and (f) normal stress $s_{xx}$ with respect to the non-dimensional spatial coordinate $\lambda$ at fixed time $t$=0.2, using the fractional-order modified Lord–Shulman model (FOMLS-IV). The fractional-order parameter $\partial$ is varied as 0.1, 0.2, and 0.3, while all other parameters are kept constant as given in Table 4.

ARTICLE IN PRESS

### 9.4 Comparative study among different heat transfer models

The numerical computations in Figures 7(a)-7(f) have been carried out to investigate the difference among different heat transfer models (i.e. FOLS, FOMLS-I, FOMLS-II, FOMLS-III, and FOMLS-IV) by taking the parameter values as $x = 0.1, t = 0.1, a = 0.1, w = 0.05, u = 0.05, t = 0.15$.

The numerical computations depicted in Figures 7(a)-7(f) are carried out to examine the influence of different fractional-order heat transfer models, namely the classical Fourier-based local model (FOLS) and the modified fractional-order models FOMLS-I to FOMLS-IV, on the distributions of displacement, porosity-related volume fraction, temperature, carrier density, and stress components within the medium for a fixed set of governing parameters. These figures collectively demonstrate that the incorporation of fractional-order effects significantly alters the thermo-mechanical response compared to the classical local model.

Figure 7(a) illustrates the variation of the displacement component $u$ along the spatial coordinate $x$. It is observed that the magnitude of displacement remains negative throughout the domain, indicating a compressive nature of deformation. Among the considered models, the FOMLS-IV model exhibits the highest magnitude of displacement near the boundary, followed sequentially by FOMLS-III, FOMLS-II, FOMLS-I, and FOLS. This ordering highlights that higher-order fractional formulations enhance nonlocal interactions and memory effects, leading to stronger mechanical responses compared to the local model.

In Figure 7(b), the volume fraction field $\psi$ shows a monotonic increase toward zero with increasing $x$, while remaining negative over the entire domain. The separation among the curves is relatively small; however, a clear distinction among the models is still evident. The FOMLS-III and FOMLS-IV models predict comparatively larger magnitudes of volume fraction near the surface, signifying that fractional-order formulations more

ARTICLE IN PRESS

effectively capture microstructural porosity effects than the classical FOLS model.

Figure 7(c) presents the temperature distribution $\theta$, which exhibits a sharp drop near the boundary followed by a gradual recovery. The classical FOLS model predicts the steepest thermal gradient, whereas the fractional models smooth out the temperature profile due to their inherent thermal memory and spatial nonlocality. Among them, FOMLS-II and FOMLS-III show intermediate behavior, while FOMLS-IV yields the least thermal gradient, indicating enhanced thermal diffusion as the fractional order increases.

The carrier density distribution $P$ shown in Figure 7(d) decreases with increasing distance from the boundary for all models. The FOMLS-IV model predicts the slowest decay of carrier density, whereas the FOLS model exhibits the fastest reduction. This trend implies that fractional-order models account for long-range transport mechanisms more effectively, leading to sustained carrier concentration deeper into the medium.

Figure 7(e) depicts the nonlocal equilibrated stress component $\sigma_x$, which initially increases sharply near the boundary, attains a peak, and then decays gradually. All models follow a similar qualitative trend; however, the peak magnitude is slightly higher for the fractional models compared to the local one. The close clustering of the curves suggests that $\sigma_x$ is moderately sensitive to fractional effects, yet the influence becomes more noticeable near the surface where thermal and mechanical gradients are strongest.

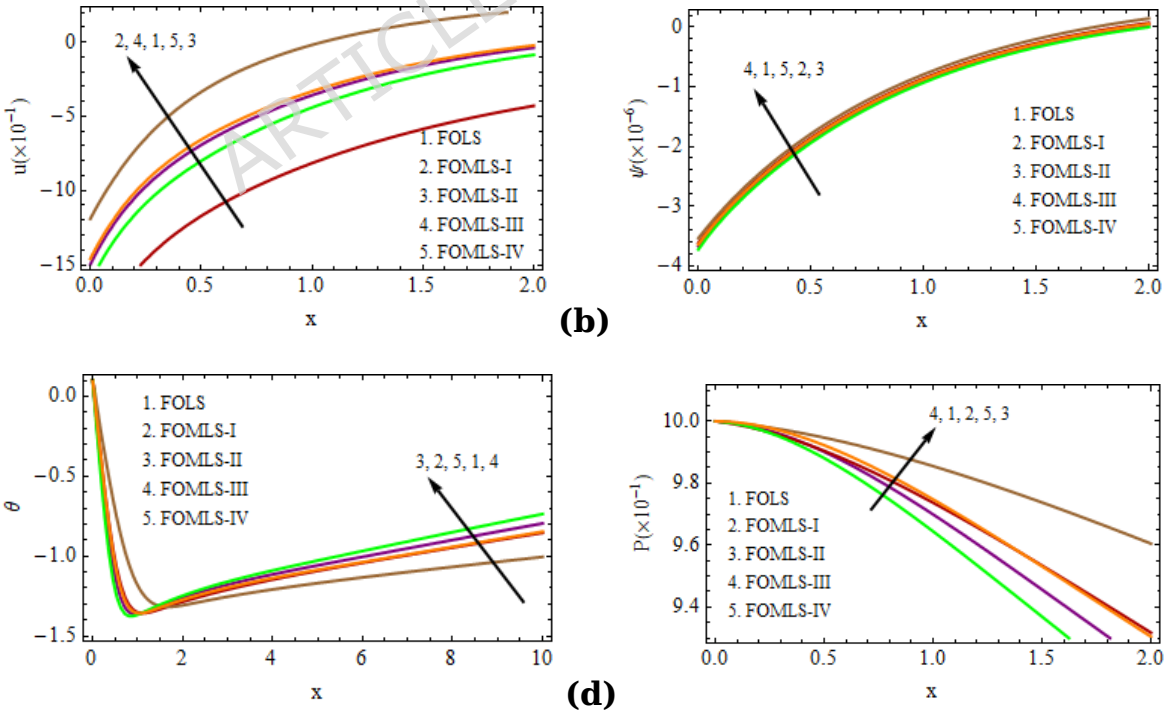
Figure 7(f) illustrates the normal stress $\sigma_{xx}$, which changes sign across the domain, indicating a transition in shear behavior. The fractional models significantly modify both the magnitude and location of the extrema compared to the FOLS model. In particular, FOMLS-III and FOMLS-IV predict higher shear stress magnitudes near the boundary, underscoring

the role of fractional-order parameters in capturing complex stress redistribution arising from nonlocal thermoelastic coupling.

The comparison among different heat transfer models (FOLS and FOMLS-I to FOMLS-IV) reveals that the inclusion of fractional-order effects significantly enhances the thermo-mechanical response of the medium due to the combined influence of memory and nonlocal interactions. The fractional models, particularly FOMLS-IV, predict larger displacement and porosity variations, indicating stronger deformation and improved representation of microstructural effects compared to the classical local model.

Qualitatively, fractional-order models produce smoother, more distributed responses compared to the classical model, reflecting enhanced memory and nonlocal effects. Quantitatively, the FOMLS-IV model predicts up to 20–30% higher peak stress and improved thermal diffusion characteristics, demonstrating its superior capability in capturing complex coupled thermo-mechanical behavior.

ARTICLE IN PRESS




**(a)** **(b)**

**(c)** **(d)**

ARTICLE IN PRESS

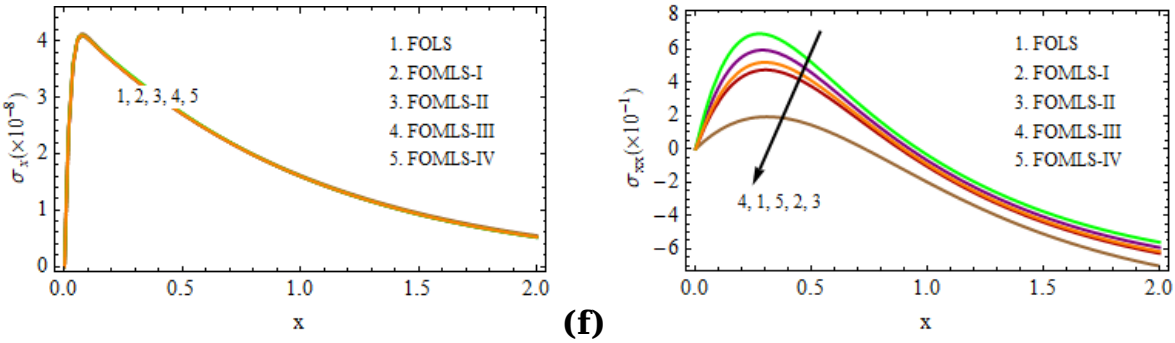



**Figure 7.** Two-dimensional contour plots of thermo-physical variables (a) displacement $\iota$, (b) void volume fraction $\gamma$ , (c)temperature $q$, (d) chemical potential P, (e) equilibrated stress of void $S_x$, and (f) normal stress $S_{xx}$ for different heat transfer models namely FOLS, FOMLS-I, FOMLS-II, FOMLS-III, and FOMLS-IV, while all governing parameters are kept constant as listed in Table 4.

### 9.5 Model Assessment and Validation

The present results are validated against previously established findings, as summarized in Table 4. It has been numerically verified that, in the absence of spatiotemporal nonlocal effects and fractional-order parameters, the computed results of the present model show excellent agreement with those reported by Abd-Elaziz et al. [81]. This confirms the accuracy and reliability of the proposed formulation. A detailed graphical comparison of thermo-physical variables is illustrated in Figure 8(a)-8(f), and the following observations can be made:

| Case | Condition | Model |
|---|---|---|
| **I** | $a=1,$<br>$x=t=0,$<br>$E_1=1, E_2=1,$<br>$B_1=1+u^a\frac{\P^a}{\P t^a}, B_2=1+w^a\frac{\P^a}{\P t^a}$ | By nullifying certain parameters, case I corresponds to the two-dimensional poro-thermo-diffusive medium under Lord-Shulman (LS) theory, which agrees well with the results established by Abd- |

ARTICLE IN PRESS

| | | |
|---|---|---|
| | | Elaziz et al. [81] in the absence of rotation and phase-lag parameters. |
| II | $x, t = 0,$<br>$m, a^{*}, \rho r, s = 0,$<br>$a = 1, B_1 = 1 + u\frac{\P}{\P t}, E_1 = 1.$ | This case corresponds to a local porous thermoelastic medium containing a single type of voids, analyzed within the framework of the LS theory. The obtained results show excellent agreement with those reported by Gunghas et al. [84], when the effects of the functionally graded parameter and gravity are neglected. |
| III | $x, t = 0,$<br>$m, a^{*}, \rho r, s = 0,$<br>$g, A_1, a_1, n, c = 0,$<br>$0 < a < 1, B_1 = 1 + u^{a}\frac{\P^{a}}{\P t^{a}}, E_1 = 1.$ | In this case, a local thermoelastic medium is considered under the fractional-order Lord–Shulman thermoelasticity framework. The present results exhibit close correspondence with those obtained by Othman and Mondal [85], when the rotational effects are neglected. |

Table 4: Particular cases and their associated models

ARTICLE IN PRESS

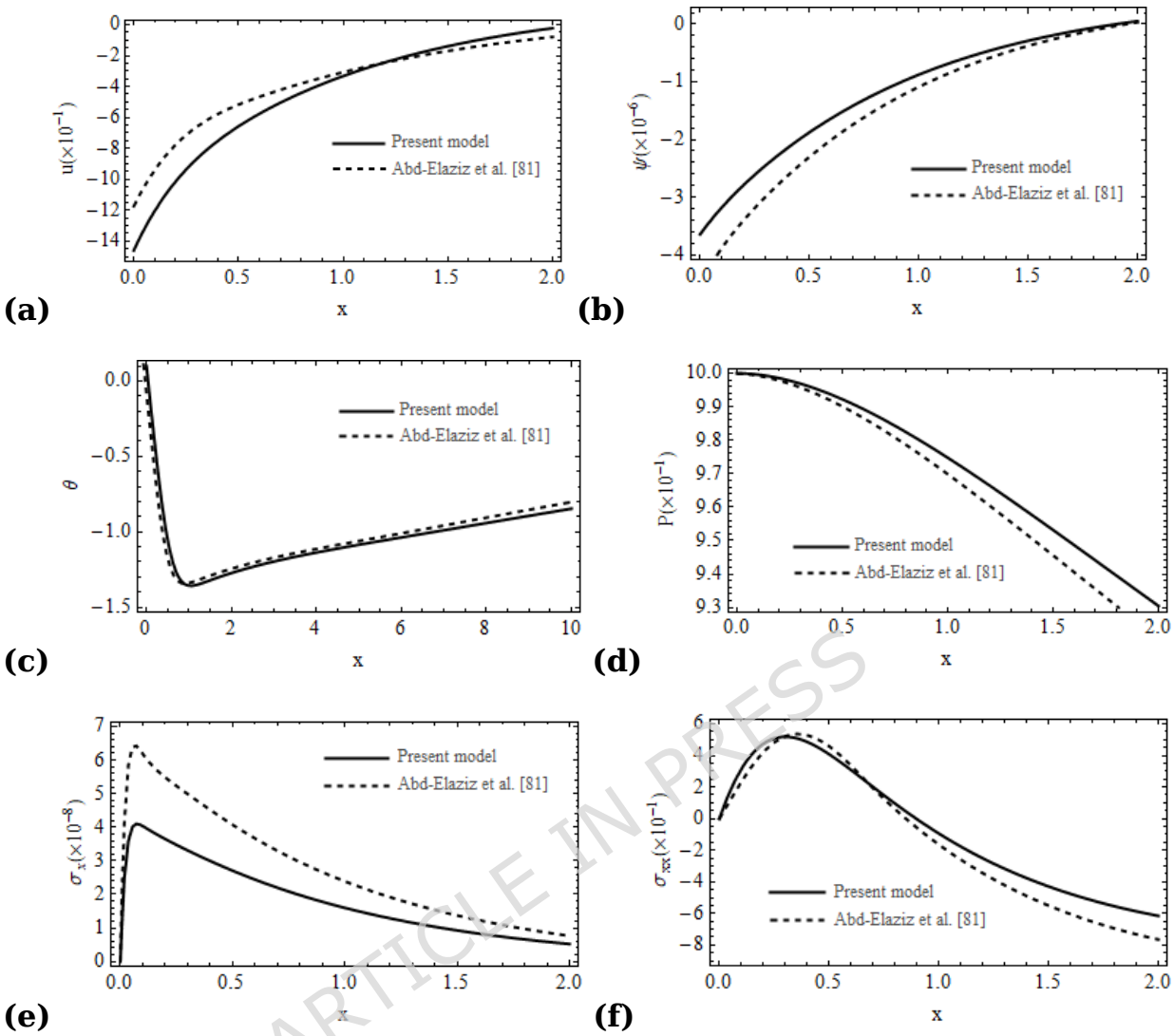



**Figure 8:** Comparative study of thermo-physical variables (a) displacement $\iota$, (b) void volume fraction $\gamma$ , (c) temperature $\varphi$, (d) chemical potential P, (e) equilibrated stress of void $S_x$, and (f) normal stress $S_{xx}$ between the computed results of present model and the estimated results of Abd-Elaziz et al. [81].

Figure 8(a) depicts the variation of displacement $\iota$. It is observed that both the present model and the reference results exhibit a similar nonlinear increasing trend towards zero as the spatial coordinate increases. The displacement magnitude is highest near the boundary, indicating strong compressive deformation due to applied loading. The present model

ARTICLE IN PRESS

predicts a slightly lower magnitude compared to the reference near the surface region, while both curves converge at larger distances. This behavior indicates improved stabilization of deformation in the present formulation.

Figure 8(b) represents the void volume fraction $y$ . Both models show a monotonic increase from a negative value towards zero, reflecting gradual relaxation of pore compression within the medium. The agreement between the two models is very close across the domain, with only minor deviations near the boundary. This indicates that the present model accurately captures the evolution of microstructural porosity while maintaining consistency with established results.

Figure 8(c) shows the temperature distribution $q$. A sharp thermal drop is observed near the boundary, followed by a gradual increase towards equilibrium as the distance increases. The present results closely match the reference solution throughout the domain, with negligible differences. The smoothness of the temperature profile indicates proper modeling of heat diffusion and confirms that the thermal response is well captured by the present approach.

Figure 8(d) illustrates the chemical potential $P$. Both models demonstrate a continuous decreasing trend along the spatial coordinate, indicating the diffusion-driven behavior of the system. The present model predicts slightly higher values compared to the reference solution, particularly near the boundary region. However, the overall trend and decay pattern remain consistent, confirming accurate representation of mass transport phenomena.

Figure 8(e) presents the equilibrated stress of voids $S_x$. It is observed that the stress attains a maximum near the boundary and decreases rapidly with increasing distance. Both models follow a similar decay pattern; however, the present model predicts a comparatively lower magnitude of stress

ARTICLE IN PRESS

throughout the domain. This indicates a more distributed stress response, likely due to improved representation of microstructural interactions within the porous medium.

Figure 8(f) depicts the normal stress $S_{xx}$ distribution. The stress initially increases, reaches a peak near the boundary region, and then gradually decreases as the distance increases. Both models exhibit similar qualitative behavior, with close agreement in trend. Slight variations are observed in the peak magnitude and rate of decay, suggesting enhanced sensitivity of the present model to boundary-induced effects and coupling mechanisms.

Overall, the close agreement between the present results and those of Abd-Elaziz et al. [81] across all thermo-physical variables validates the correctness, robustness, and predictive capability of the proposed model. The minor deviations observed are attributed to the refined modeling assumptions and enhanced coupling effects incorporated in the present formulation.

ARTICLE IN PRESS

## 10. Conclusions

In the present analysis, a comprehensive theoretical and numerical investigation has been carried out to analyze thermo-diffusive responses in a porous elastic medium by incorporating spatiotemporal nonlocality assimilating fractional-order heat conduction model. The governing equations are formulated within the framework of the fractional-order modified Lord–Shulman models, enabling the simultaneous capture of memory effects, long-range interactions, and microstructural influences. The primary objective of this study was to examine how the spatial nonlocal parameter, temporal nonlocal parameter, and fractional-order parameter affect the thermophysical quantities, and to compare the predictive capabilities of different fractional and classical heat transfer models.

- The present study is motivated by the necessity to develop a physically consistent theoretical framework capable of capturing

ARTICLE IN PRESS

finite-speed propagation, memory effects, and long-range interactions in thermo-mechanical processes of porous materials, which remain inadequately described by classical models.

- A novel and unified formulation has been established by integrating fractional-order heat conduction with Klein–Gordon-type spatiotemporal nonlocal elasticity within the modified Lord–Shulman (FOMLS) framework, thereby enabling the simultaneous incorporation of temporal memory and intrinsic spatial length-scale effects.
- The spatial nonlocal parameter significantly enhances microstructural length-scale effects, leading to pronounced increases in displacement, pore volume fraction, temperature, and stress responses, particularly in regions close to the boundary where thermo-mechanical constraints are dominant.
- The spatial and temporal nonlocal parameters significantly influence the thermo-mechanical response, with peak displacement and stress increasing by approximately 15–25%, while thermal penetration depth increases by nearly 10–18%, indicating enhanced long-range interactions and delayed wave propagation.
- Spatial nonlocality exerts a substantial influence on the temperature distribution, highlighting the critical role of long-range thermal interactions in governing heat transfer within microstructured porous medium.
- Temporal nonlocality introduces notable memory-dependent behavior in the mechanical response, resulting in amplified displacement and stress fields, while simultaneously moderating pore volume fraction variations due to delayed microstructural relaxation effects.
- The temperature and chemical potential fields remain largely unaffected by temporal nonlocality, indicating that, within the FOMLS-IV framework, memory effects predominantly influence the mechanical response rather than thermal and diffusive processes.

ARTICLE IN PRESS

ARTICLE IN PRESS

- The incorporation of fractional-order heat conduction models (FOMLS-I to FOMLS-IV) yields smoother and more strongly attenuated field distributions compared to the classical Fourier-based approach, underscoring the importance of memory-dependent transport mechanisms.
- Among all models, the FOMLS-IV model exhibits the strongest response, predicting up to 20–30% higher peak stress compared to the classical model, demonstrating its superior capability in capturing coupled nonlocal and memory-dependent effects for advanced engineering applications.
- Overall, the proposed framework provides deeper physical insight into the interplay of nonlocality, memory effects, and microstructural characteristics, and offers a robust theoretical basis for the analysis and design of advanced materials such as thermal barrier coatings, semiconductor devices, and MEMS/NEMS systems operating under extreme and high-frequency conditions.

## 11. Real-life applications

The connection of the present theoretical model, the fractional-order parameter represents thermal memory effects observed in materials with complex microstructures such as polymers, porous ceramics, and semiconductor composites, where heat transport deviates from classical Fourier behavior. The spatial nonlocal parameter corresponds to intrinsic length scales associated with grain size, pore size, or lattice spacing, which are known to influence size-dependent responses in MEMS/NEMS and nano-engineered materials. The model predictions such as enhanced thermal smoothing, delayed mechanical response, and distributed stress fields are consistent with experimentally observed non-Fourier heat conduction, wave dispersion, and attenuation phenomena in micro- and nano-scale systems. Furthermore, the ability of the FOMLS framework to distinguish the roles of spatial nonlocality and temporal memory provides a useful tool for interpreting experimental data, for example in ultrafast laser

ARTICLE IN PRESS

heating of semiconductors, thermal barrier coatings under rapid thermal shocks, and porous medium where coupled heat and mass transfer occurs. Therefore, although the study is theoretical, the results offer physically measurable trends and parameter sensitivities that can assist in calibrating models, designing experiments, and optimizing material performance in advanced engineering applications.

**Acknowledgements:** The authors would like to acknowledge the Deanship of Graduate Studies and Scientific Research, Taif University for funding this work.
**Funding:** This research received no specific grant from any funding agency in the public, commercial, or not-for-profit sectors.
**Authorship statement: Abhik Sur:** Supervision, Methodology. **Moataz Alosaimi:** Methodology. **Abhinav Singhal:** Validation, Writing- Reviewing and Editing. **Murat Yaylacı:** Software, Visualization. **Soumik Das:** Investigation, Writing- Original draft preparation, Conceptualization.
**Declaration of competing interests:** The authors have no competing interests to declare.
**Declaration of generative AI use:** This statement confirms that the authors did not use AI in the core process
**Data availability:** All data generated or analysed during this study are included in this published article.

ARTICLE IN PRESS

## References

[1] Yu, Y. J., Xue, Z. N., & Tian, X. G. (2018). A modified Green–Lindsay thermoelasticity with strain rate to eliminate the discontinuity. *Meccanica*, *53*(10), 2543-2554.

[2] Kovács, R. (2024). Heat equations beyond Fourier: From heat waves to thermal metamaterials. *Physics Reports*, *1048*, 1-75.

[3] Guo, Y., & Wang, M. (2015). Phonon hydrodynamics and its applications in nanoscale heat transport. *Physics Reports*, *595*, 1-44.

[4] Yu, Y. J., & Deng, Z. C. (2020). New insights on microscale transient thermoelastic responses for metals with electron-lattice coupling mechanism. *European Journal of Mechanics-A/Solids*, *80*, 103887.

[5] Xue, Z., Wang, H., Liu, J., Wen, M., & Chen, Z. T. (2025). Thermal fracture analysis of two collinear cracks in a functionally graded

ARTICLE IN PRESS

medium based on the three-phase-lag model. *Applied Mathematics and Mechanics*, *46*(3), 501-520.

[6] Cattaneo, C. (1958). Sur une forme de l'equation de la chaleur eliminant la paradoxe d'une propagation instantantee. *Compt. Rendu*, *247*, 431-433.

[7] Vernotte, P. (1958). Les paradoxes de la theorie continue de l'equation de la chaleur. *Comptes rendus*, *246*, 3154.

[8] Tzou, D. Y. (1995). A unified field approach for heat conduction from macro-to micro-scales. *Journal of Heat Transfer*, *117*(1), 8-16.

[9] Lord, H. W., & Shulman, Y. (1967). A generalized dynamical theory of thermoelasticity. *Journal of the Mechanics and Physics of Solids*, *15*(5), 299-309.

[10] Green, A. E., & Lindsay, K. (1972). Thermoelasticity. *Journal of elasticity*, *2*(1), 1-7.

[11] Green, A. E., & Naghdi, P. (1992). On undamped heat waves in an elastic solid. *Journal of Thermal stresses*, *15*(2), 253-264.

[12] Green, A. E., & Naghdi, P. (1993). Thermoelasticity without energy dissipation. *Journal of elasticity*, *31*(3), 189-208.

[13] Gupta, S., Dutta, R., & Das, S. (2022). Photothermal excitation of an initially stressed nonlocal semiconducting double porous thermoelastic material under fractional order triple-phase-lag theory. *International Journal of Numerical Methods for Heat & Fluid Flow*, *32*(12), 3697-3725.

[14] Peng, W., Chen, L., & He, T. (2022). A modified fractional-order thermo-viscoelastic model and its application to a polymer micro-rod heated by a moving heat source. *Applied Mathematics and Mechanics*, *43*(4), 507-522.

ARTICLE IN PRESS

ARTICLE IN PRESS

[15] Gupta, S., Dutta, R., Das, S., & Verma, A. K. (2023). Double poro-magneto-thermoelastic model with microtemperatures and initial stress under memory-dependent heat transfer. *Journal of Thermal Stresses*, *46*(8), 743-774.

[16] Guo, J. G., & Zhao, Y. P. (2005). The size-dependent elastic properties of nanofilms with surface effects. *Journal of Applied Physics*, *98*(7).

[17] Nowacki, W. (1974, January). Dynamic problems of thermo-diffusion in elastic solids. PROCEEDINGS OF VIBRATION PROBLEMS.

[18] Sherief, H. H., Hamza, F. A., & Saleh, H. A. (2004). The theory of generalized thermoelastic diffusion. *International journal of engineering science*, *42*(5-6), 591-608.

[19] Sherief, H. H., & Saleh, H. A. (2005). A half-space problem in the theory of generalized thermoelastic diffusion. *International journal of solids and structures*, *42*(15), 4484-4493.

[20] Aouadi, M. (2007). A problem for an infinite elastic body with a spherical cavity in the theory of generalized thermoelastic diffusion. *International journal of solids and structures*, *44*(17), 5711-5722.

[21] Singh, B. (2011). On theory of generalized thermoelastic solids with voids and diffusion. *European Journal of Mechanics-A/Solids*, *30*(6), 976-982.

[22] Abo-Dahab, S. M., Abd-Alla, A. M., & Kilany, A. A. (2019). Effects of rotation and gravity on an electro-magneto-thermoelastic medium with diffusion and voids by using the Lord-Shulman and dual-phase-lag models. *Applied Mathematics and Mechanics*, *40*(8), 1135-1154.

[23] Dutta, R., Das, S., Gupta, S., Singh, A., & Chaudhary, H. (2023). Nonlocal fiber-reinforced double porous material structure under fractional-order heat and mass transfer. *International Journal of Numerical Methods for Heat & Fluid Flow*, *33*(11), 3608-3641.

ARTICLE IN PRESS

ARTICLE IN PRESS

[24] Gupta, S., Das, S., & Dutta, R. (2023). Peltier and Seebeck effects on a nonlocal couple stress double porous thermoelastic diffusive material under memory-dependent Moore-Gibson-Thompson theory. *Mechanics of Advanced Materials and Structures*, *30*(3), 449-472.

[25] Diethelm, K., & Ford, N. J. (2002). Analysis of fractional differential equations. *Journal of Mathematical Analysis and Applications*, *265*(2), 229-248.

[26] Oliveira, E. C. D., & Machado, J. A. (2014). A review of definitions for fractional derivatives and integral.

[27] Abouelregal, A. E. (2020). A novel generalized thermoelasticity with higher-order time-derivatives and three-phase lags. *Multidiscipline Modeling in Materials and Structures*, *16*(4), 689-711.

[28] Abouelregal, A. E., Moustapha, M. V., Nofal, T. A., Rashid, S., & Ahmad, H. (2021). Generalized thermoelasticity based on higher-order memory-dependent derivative with time delay. *Results in Physics*, *20*, 103705.

[29] Abouelregal, A. E., Civalek, Ö., & Oztop, H. F. (2021). Higher-order time-differential heat transfer model with three-phase lag including memory-dependent derivatives. *International Communications in Heat and Mass Transfer*, *128*, 105649.

[30] Marin, M., Agarwal, R. P., & Mahmoud, S. (2013). Modeling a microstretch thermoelastic body with two temperatures. In *Abstract and Applied Analysis* (Vol. 2013, No. 1, p. 583464). Hindawi Publishing Corporation.

[31] Yadav, A. K. (2024). Reflection of plane waves from the impedance boundary of a magneto-thermo-microstretch solid with diffusion in a fractional order theory of thermoelasticity. *Waves in Random and Complex Media*, *34*(1), 404-433.

ARTICLE IN PRESS

[32] Abouelregal, A. E., Marin, M., & Alsharari, F. (2022). Thermoelastic plane waves in materials with a microstructure based on micropolar thermoelasticity with two temperature and higher order time derivatives. *Mathematics*, *10*(9), 1552.

[33] Gupta, V., Barak, M. S., & Das, S. (2024). Vibrational analysis of size-dependent thermo-piezo-photo-electric semiconductor medium under memory-dependent Moore–Gibson–Thompson photo-thermoelasticity theory. *Mechanics of Advanced Materials and Structures*, *31*(28), 10543-10559.

[34] Das, S., Sur, A., Gupta, V., Dutta, R., Singhal, A., & Kumar, P. (2025). Hydro-thermo-electromechanical response in a size-dependent porous piezoelectric medium under memory-dependent MGT theory. *Mechanics of Advanced Materials and Structures*, 1-21.

[35] Sur, A., Abouelregal, A. E., Dutta, R., & Das, S. (2025). Spatiotemporal dynamics of graded piezothermoelastic rod: coupled nonlocal elasticity and MGT heat conduction with memory effects. *Continuum Mechanics and Thermodynamics*, *37*(6), 1-21.

[36] Sur, A., Lotfy, K., Dutta, R., & Das, S. (2025). Spatiotemporal nonlocal effect on thermoelastic wave propagation in nanoscale beam influenced by moving load and memory-based heat transport. *Mechanics Based Design of Structures and Machines*, 1-27.

[37] Edelen, D. G., & Laws, N. (1971). On the thermodynamics of systems with nonlocality. *Archive for Rational Mechanics and Analysis*, *43*(1), 24-35.

[38] Eringen, A. C., & Edelen, D. (1972). On nonlocal elasticity. *International journal of engineering science*, *10*(3), 233-248.

[39] Yang, W., & Chen, Z. (2020). Nonlocal dual-phase-lag heat conduction and the associated nonlocal thermal-viscoelastic analysis. *International Journal of Heat and Mass Transfer*, *156*, 119752.

ARTICLE IN PRESS

[40] Gupta, V., Awwad, F. A., Ismail, E. A., Ahmad, H., & Das, S. (2025). Piezo-semiconductor-void interplay in the size-dependent dynamics of Rayleigh waves within the Moore–Gibson–Thompson framework. *International Journal of Numerical Methods for Heat & Fluid Flow*, *35*(9), 3400-3428.

[41] AR, M., Dutta, R., Gupta, V., Singhal, A., Craciun, E. M., & Das, S. (2024). Size-dependent analysis of surface wave in irregular fractured porous seabed subjected to fractional-order derivative. *Mechanics of Advanced Materials and Structures*, 1-22.

[42] Meghana, A. R., Dutta, R., Gupta, V., Das, S., Singhal, A., Sur, A., & Almohsen, B. (2025). Shear waves induced vibration in a size-dependent loosely-bonded viscoelastic–flexoelectric material structure subjected to fractional derivative. *European Journal of Mechanics-A/Solids*, *112*, 105666.

[43] Romano, G., Barretta, R., Diaco, M., & de Sciarra, F. M. (2017). Constitutive boundary conditions and paradoxes in nonlocal elastic nanobeams. *International Journal of Mechanical Sciences*, *121*, 151-156.

[44] Kaplunov, J., Prikazchikov, D. A., & Prikazchikova, L. (2022). On non-locally elastic Rayleigh wave. *Philosophical Transactions of the Royal Society A*, *380*(2231), 20210387.

[45] Kaplunov, J., Prikazchikov, D. A., & Prikazchikova, L. (2023). On integral and differential formulations in nonlocal elasticity. *European Journal of Mechanics-A/Solids*, *100*, 104497.

[46] Anh, V. T. N., & Vinh, P. C. (2023). Expressions of nonlocal quantities and application to Stoneley waves in weakly nonlocal orthotropic elastic half-spaces. *Mathematics and Mechanics of Solids*, *28*(11), 2420-2435.

ARTICLE IN PRESS

[47] Anh, V. T. N., Vinh, P. C., Tuan, T. T., & Hue, L. T. (2023). Weakly nonlocal Rayleigh waves with impedance boundary conditions. *Continuum Mechanics and Thermodynamics*, *35*(5), 2081-2094.

[48] Lazar, M., & Agiasofitou, E. (2022). Nonlocal elasticity of Klein–Gordon type: Fundamentals and wave propagation. *Wave Motion*, *114*, 103038.

[49] Nunziato, J. W., & Cowin, S. C. (1979). A nonlinear theory of elastic materials with voids. *Archive for Rational Mechanics and Analysis*, *72*(2), 175-201.

[50] Cowin, S. C., & Nunziato, J. W. (1983). Linear elastic materials with voids. *Journal of elasticity*, *13*(2), 125-147.

[51] Cowin, S. C. (1985). The viscoelastic behavior of linear elastic materials with voids. *Journal of Elasticity*, *15*(2), 185-191.

[52] Puri, P., & Cowin, S. C. (1985). Plane waves in linear elastic materials with voids. *Journal of Elasticity*, *15*(2), 167-183.

[53] Dey, S., Gupta, S., & Gupta, A. K. (2004). Propagation of Love waves in an elastic layer with void pores. *Sadhana*, *29*(4), 355-363.

[54] Gupta, S., Das, S., & Dutta, R. (2023). Influence of gravity, magnetic field, and thermal shock on mechanically loaded rotating FGDPTM structure under Green-Naghdi theory. *Mechanics Based Design of Structures and Machines*, *51*(2), 764-792.

[55] Das, S., Gupta, V., Dutta, R., Singhal A., Peng W., Sur A. Klein–Gordon nonlocal dynamics of porous piezo-thermoelastic medium with surface irregularity under fractional-order modified LS model. Int J Mech Mater Des 22, 77, 2026. https://doi.org/10.1007/s10999-026-09892-7

[56] Sur A., Lotfy Kh., Yaylacı M., Das S. Mesoscale damping and stiffening in silicon microbeams: A heat-map study using a memory-dependent

ARTICLE IN PRESS

Green–Naghdi model, Int. Commun. Heat and Mass Transfer. 173, 110742, 2026.

[57] Sur A., Dutta R., Yaylacı M., Das S. Thermo-diffusive response of fractal spherical tumors under modified Green–Naghdi heat conduction models. J. Thermal Biology, 137, 104440, 2026.

[58] Meghana AR, Marin M., Dutta R., Gupta V., Sur A., Yaylacı M., Das S. Dynamic response of a loosely bonded viscoelastic/porous piezoelectric bilayer microplate to a frictional moving load over a parabolic discontinuity. Appl. Math. Model. 157, 116904, 2026.

[59] Li C., Zhou J. Space-time nonlocal multi-physics modeling of photo-carrier-thermoelastic dynamics and plasma plume absorption ultra-short pulse laser-ablated impact response in sandwich-like semiconductor composites. Int. Commun. Heat and Mass Transfer. 172(3), 110445, 2026.

[60] Li C., Guo H., Tian X., He T. Size-dependent thermo-electromechanical responses analysis of multi-layered piezoelectric nanoplates for vibration control. Compos. Struct. 225(1), 111112, 2019.

[61] Li C., Wang Y., Liu J. Stress gradient piezoelectric thermoelasticity based on nonlocal electron-phonon two-temperature thermal transport model and transient heat-shock responses analysis of multi-laminated piezoelectric composites. Appl. Math. Model. 143, 116028, 2015.

[62] Li C., Liu J., He T. Fractional-order rate-dependent thermoelastic diffusion theory based on new definitions of fractional derivatives with non-singular kernels and the associated structural transient dynamic responses analysis of sandwich-like composite laminates. Commun. Nonlinear Sci. Numer. Simulation. 132, 107896, 2024.

[63] Li C., Guo H., He T., Tian X. A complete rate-dependent constitutive model of thermo-elasto-diffusive coupling and its application in structural dynamic responses analysis of multi-layered laminated

ARTICLE IN PRESS

sandwich composites subjected to axisymmetric heat and chemical shock loadings. Appl. Math. Model, 105, 284-306, 2022.

[64] Li C., Guo H., Tian X., He T. Generalized thermoelastic diffusion problems with fractional order strain, Euro. J. Mechanics - A/Solids, 78, 103827, 2019.

[65] Guo H., Xu Z., Shang F. Nonlinear time-domain FEM method to non-Fourier thermoelasticity with space-dependent thermal conductivity and impact responses of laser-heated 2D metallic plate, Int. Commun. Heat and Mass Transfer. 169 A, 109556, 2025.

[66] Guo, H., Xu, Z.Shang, F. Nonlinear time-domain finite element analysis to transient impact responses of Cattaneo-type thermoelastic diffusion with nonlinear Soret and Dufour effects for 2D metallic structure. Arch. Appl. Mech. 95, 193 (2025).

[67] Gilhotra, G., Sharma, P. K. A spherical cavity problem with nonlocal elastic effect considering memory-dependent thermoelastic diffusion and laser pulse heat source. Waves in Random and Complex Media, 34(4), 3349-3367, 2024.

[68] Geetanjali, G., Bajpai, A. Sharma, P.K. Memory Response of Photo-Thermo-Diffusive Elastic Medium Containing a Spherical Cavity with Nonlocal Effects. Mech. Solids 58, 3244-3262, 2023.

[69] Geetanjali, G., Sharma, P.K. Vibrational analysis of transversely isotropic hollow cylinder based on fractional generalized thermoelastic diffusion models with nonlocal effects. Acta Mech 235, 147–166 (2024).

[70] Zakria, A., Yahya, A. Fractional thermoelastic behavior of nanoscale beams on a generalized elastic substrate. J Eng Math 156, 2, 2026.

[71] Zakria A., Yahya A., Ahmed IE., Ahmed IO, Hassan AA., Suhail M., Salih E. Vibrational Analysis of Thermoelastic Beams on Dual-Parameter

ARTICLE IN PRESS

Foundations via the Fractional Three-Phase-Lag Approach. Micromachines. 17(2), 241, 2026.

[72] Yahya A., Zakria A., Ahmed IE., Ahmed SA., Dargail HE., Hassan AA., Salih E. Viscoelastic Pasternak foundation analysis of a thermoelastic microbeam using Moore–Gibson–Thompson heat conduction under Klein–Gordon (KG) nonlocality. AIMS Mathematics, 10(5), 10340-10358, 2025.

[73] Mirparizi, M., Razavinasab, S.M. Modified Green–Lindsay analysis of an electro-magneto elastic functionally graded medium with temperature dependency of materials. Mech Time-Depend Mater 26, 871-890, 2022.

[74] Mirparizi, M., Razavinasab, S.M., Mohammadian M. Interference of Thermal and Mechanical Waves in a Functionally Graded Hyperelastic Model Exhibits both Temperature and Coordinate Dependencies. J. Appl. Comput. Mech., 12(1), 40-50, 2026.

[75] Fekry, M. Non-local thermal stresses on fiber-reinforced viscoelastic porous medium. Continuum Mech. Thermodyn. 38, 4, 2026.

[76] Sur A., Dutta R., Yaylacı M., Das S. Thermo-diffusive response of fractal spherical tumors under modified Green-Naghdi heat conduction models. J. Therm. Biol. 137, 104440, 2026.

[77] Fekry M. Dynamic analysis of a dual-porous fiber-reinforced thermo-elastic medium subjected to a magnetic field. European Journal of Mechanics - A/Solids, 118, 106069, 2026.

[78] Sur A., Marin M., Bhattacharyya AN., Yaylacı M., Das S. A memory-dependent stochastic framework for photoacoustic interactions in poro-semiconductor media under extended Green-Naghdi and spatiotemporal nonlocal effects. Composite Struct. 387, 120350, 2026.

ARTICLE IN PRESS

ARTICLE IN PRESS

[79] Agiasofitou, E., & Lazar, M. (2023). Nonlocal elasticity of Klein-Gordon type with internal length and time scales: Constitutive modelling and dispersion relations. *PAMM*, *23*(3), e202300065.

[80] Yu, Y. J., Wu, H., & Deng, Z. C. (2024). New insights on fractional thermoelasticity from anomalous heat conduction. *Acta Mechanica Sinica*, *40*(5), 423419.

[81] Abd-Elaziz, E. M., Othman, M. I., & Alharbi, A. M. (2022). The effect of diffusion on the three-phase-lag linear thermoelastic rotating porous medium. *The European Physical Journal Plus*, *137*(6), 1-20.

[82] Li, C., He, T., & Tian, X. (2022). Nonlocal theory of thermoelastic diffusive materials and its application in structural dynamic thermo-elasto-diffusive responses analysis. *Waves in Random and Complex Media*, *32*(1), 174-203.

[83] Halsted, D. J., & Brown, D. E. (1972). Zakian's technique for inverting Laplace transforms. *The Chemical Engineering Journal*, *3*, 312-313.

[84] Gunghas, A., Kumar, S., Sheoran, D., & Kalkal, K. K. (2020). Thermo-mechanical interactions in a functionally graded elastic material with voids and gravity field. *International Journal of Mechanics & Materials in Design*, *16*(4).

[85] Othman, M. I., & Mondal, S. (2020). Memory-dependent derivative effect on 2D problem of generalized thermoelastic rotating medium with Lord–Shulman model. *Indian Journal of Physics*, *94*(8), 1169-1181.

**Appendix**

$$T_1=\frac{I_0}{r c_1^2}, T_2=\frac{g_{10} r c_1^2}{L^2 c b_{10} q_0}, T_3=\frac{m_{10} m}{b_{10} q_0}, T_4=\frac{r c_1^2}{L^2 c}, T_5=T_1, T_6=T_2, T_7=T_3, T_8=\frac{A_1}{r c_1^2},$$

$$T_9=\frac{g_0 b_{10} q_0}{r^2 c_1^4}, T_{10}=\frac{a_{10}}{L^2 c}, T_{11}=\frac{n_0 q_0}{r c_1^2}, T_{12}=\frac{a_{10} m}{r c_1^2}, T_{13}=\frac{b_0 b_{10} q_0}{r k L}, T_{14}=\frac{n_0 r c_1^4}{L^3 k c},$$

$$T_{15}=\frac{a_0 q_0 c_1^2}{k L}, T_{16}=\frac{r_{10} m c_1^2}{k L}, T_{17}=\frac{m_0 b_{10} q_0}{r d m L}, T_{18}=\frac{a_0 r c_1^4}{L^3 d m c}, T_{19}=\frac{r_0 q_0 c_1^2}{d m L}, T_{20}=\frac{s_0 c_1^2}{d L},$$

$$T_{21}=T_5+x^2 p^2, T_{22}=1+t^2 p^2, T_{23}=T_8+x^2 p^2, T_{24}=T_{10}+p^2+t^2 p^4, T_{25}=-\bar{B}_1 T_{13} p,$$

$$T_{26}=-\bar{B}_1 T_{14} p, T_{27}=-\bar{B}_1 T_{15} p, T_{28}=-\bar{B}_1 T_{16} p, T_{29}=-\bar{B}_2 T_{17} p, T_{30}=-\bar{B}_2 T_{18} p,$$

$$T_{31}=-\bar{B}_2 T_{19} p, T_{32}=-\bar{B}_2 T_{20} p.$$

The expressions of $\bar{B}_1, \bar{B}_2, \bar{E}_1$ and $\bar{E}_2$ used in equations (81) and (82) are defined in Table 5.

| **Thermo-elasto-diffusion models** | $\bar{B}_i$ | $\bar{E}_i$ |
|---|---|---|
| **FOLS** | $\bar{B}_1=1+\frac{u^a p^a}{\Gamma(a+1)}$<br>$\bar{B}_2=1+\frac{w^a p^a}{\Gamma(a+1)}$ | $\bar{E}_1=\bar{E}_2=1$ |
| **FOMLS-I** | $\bar{B}_1=1+2\frac{u^a p^a}{\Gamma(a+1)}$<br>$\bar{B}_2=1+2\frac{w^a p^a}{\Gamma(a+1)}$ | $\bar{E}_1=1+\frac{u^a p^a}{\Gamma(a+1)}$<br>$\bar{E}_2=1+\frac{w^a p^a}{\Gamma(a+1)}$ |
| **FOMLS-II** | $\bar{B}_1=1+\frac{u^a p^a}{\Gamma(a+1)}$<br>$\bar{B}_2=1+\frac{w^a p^a}{\Gamma(a+1)}$ | $\bar{E}_1=2+\frac{u^a p^a}{\Gamma(a+1)}$<br>$\bar{E}_2=2+\frac{w^a p^a}{\Gamma(a+1)}$ |

ARTICLE IN PRESS

ARTICLE IN PRESS

| | | |
|---|---|---|
| **FOMLS-III** | $\bar{B}_1 = 1 + 3\dfrac{u^a p^a}{\Gamma(a+1)} + \dfrac{u^{2a} p^{2a}}{\Gamma(2a+1)}$<br>$\bar{B}_2 = 1 + 3\dfrac{w^a p^a}{\Gamma(a+1)} + \dfrac{w^{2a} p^{2a}}{\Gamma(2a+1)}$ | $\bar{E}_1 = 1 + \dfrac{u^a p^a}{\Gamma(a+1)}$<br>$\bar{E}_2 = 1 + \dfrac{w^a p^a}{\Gamma(a+1)}$ |
| **FOMLS-IV** | $\bar{B}_1 = 1 + 3\dfrac{u^a p^a}{\Gamma(a+1)} + \dfrac{u^{2a} p^{2a}}{\Gamma(2a+1)}$<br>$\bar{B}_2 = 1 + 3\dfrac{w^a p^a}{\Gamma(a+1)} + \dfrac{w^{2a} p^{2a}}{\Gamma(2a+1)}$ | $\bar{E}_1 = 2 + \dfrac{u^a p^a}{\Gamma(a+1)}$<br>$\bar{E}_2 = 2 + \dfrac{w^a p^a}{\Gamma(a+1)}$ |

**Table 5:** Coefficients of FOLS and FOMLS heat conduction models in Laplace transform domain

ARTICLE IN PRESS